Charles University

Third Faculty of Medicine

Dissertation thesis

Změny morfologie bílé a šedé hmoty u pacientů s

Alzheimerovou nemocí a Schizofrenií na MRI

Altered morphology of white and gray matter in patients with

Alzheimer disease and Schizophrenia on MRI

Supervisor: Prof. Petr Zach, M.D., Ph.D.

Statement

I declare that I have prepared my thesis independently and that I have properly listed and cited all sources and literature used. I also declare that the thesis has not been used to obtain another or the same degree. I agree to the permanent storage of the electronic version of my thesis in the database of the inter-university project Theses.cz for the purpose of continuous checking of the similarity of qualifying theses.

Prague, May 20, 2023 Anastasiya Lahutsina, MD

Identification record

LAHUTSINA, Anastasiya. *Altered morphology of white and gray matter in patients with Alzheimer disease and Schizophrenia on MRI*. Prague, 2023, 141 pages. Dissertation thesis (Ph.D.). Charles University, Third Faculty of Medicine, Department of Anatomy. Prof. Petr Zach, M.D., Ph.D.

Acknowledgements

First of all, I would like to thank my supervisor Prof. Petr Zach, M.D., Ph.D., for his generous guidance, support and motivation throughout my postgraduate studies and during the preparation of this thesis.

I would like to thank Filip Španiel, M.D., Ph.D., from the team of National Institute of Mental Health, for the opportunity to be part of his research team and to participate in innovative methods in neuroscience research. I also thank all colleagues who participated in data collection and processing and made the project run, as well as the outpatient psychiatrists for their cooperation in the HYDRA data collection. I would also like to thank the team of the Department of Anatomy and the AD Centre under the leadership of Prof. Aleš Bartoš, M.D., Ph.D., for the opportunity to cooperate.

Abstrakt

Velikost a tvar závitů (gyri) a žlábků (sulci) v oblasti přední cingulární kůry (ACC), zejména sulcus cinguli (CS) a sulcus paracingularis (PCS), představuje anatomický marker vývoje nervového systému. Odchylky ve vývoji *in utero* u schizofrenie lze sledovat pomocí morfometrie CS a PCS. V této studii jsme měřili délku CS, PCS a jejich segmentů na snímcích T1 MRI u 93 pacientů s první epizodou schizofrenie a u 42 zdravých kontrol. Kromě délky sulci byla u pacientů a kontrol porovnávána také frekvence výskytu a levopravá asymetrie CS/PCS. Distribuce morfotypů CS a PCS u pacientů se lišila od kontrol. Parcelovaný typ CS3a v levé hemisféře byl u pacientů delší (53,8 ± 25,7 mm oproti 32,7 ± 19,4 mm u kontrol, $p < 0,05$), zatímco u CS3c byl u kontrol naopak dlouhý (52,5 ± 22,5 mm oproti 36,2 ± 12,9 mm, n.s. u pacientů). Neparcelovaný PCS v pravé hemisféře byl delší u pacientů ve srovnání s kontrolami (19,4 ± 10,2 mm oproti 12,1 ± 12,4 mm, $p < 0,001$). Současná přítomnost PCS1 a CS1 v levé hemisféře a do jisté míry i v pravé hemisféře tedy může svědčit o vyšší pravděpodobnosti schizofrenie.

Měření plochy nebo objemu hipokampu je v klinické praxi užitečné jako podpůrná pomůcka pro diagnostiku Alzheimerovy choroby. Vzhledem k tomu, že je časově náročné a není jednoduché, využívá se nepříliš často. Předkládáme zjednodušený protokol pro hodnocení atrofie hipokampu na základě jednoho optimálního řezu u Alzheimerovy choroby. Definovali jsme jediný optimální řez pro stanovení plochy hipokampu na magnetické rezonanci mozku (MRI) v rovině, kde mizí amygdala a je přítomen pouze hipokampus. Porovnali jsme absolutní plochu a objem hipokampu na tomto optimálním řezu mezi 40 pacienty s Alzheimerovou chorobou a 40 staršími kontrolami, spárovanými podle věku, vzdělání a pohlaví. Dále jsme tyto výsledky porovnali s výsledky vztaženými k velikosti mozku nebo lebky: plocha optimálního řezu normalizovaná k ploše mozku v přední komisuře (commissura anterior) a objem hipokampu normalizovaný k celkovému intrakraniálnímu objemu (TIV). Plochy hipokampů na jediném optimálním řezu a objemy hipokampů vlevo a vpravo v kontrolní skupině byly významně vyšší než ve skupině s AD. Normalizované hipokampální plochy a objemy vlevo a vpravo v kontrolní skupině byly významně vyšší než ve skupině s AD. Absolutní plochy a objemy hipokampů se významně nelišily od odpovídajících normalizovaných ploch hipokampů ani normalizovaných objemů hipokampů pomocí porovnání ploch na ROC analýze. Plocha hipokampu na dobře definovaném optimálním řezu MRI mozku může spolehlivě nahradit komplikované měření

objemu hipokampu. Překvapivě normalizace těchto veličin vzhledem k mozku nebo lebce nepřidává žádné významnější rozlišení mezi pacienty s Alzheimerovou chorobou a kontrolami, ani nepřináší lepší výsledky.

Zmenšení objemu struktur šedé hmoty u pacientů s Alzheimerovou chorobou je často doprovázeno asymetrickým zvýšením počtu vláken bílé hmoty, která se nacházejí v blízkosti těchto struktur. Cílem této studie bylo prozkoumat změny struktury bílé hmoty u motorických bazálních gangliích u pacientů s Alzheimerovou chorobou ve srovnání se zdravými kontrolami pomocí difuzního tenzorového zobrazování (DTI). U deseti pacientů s Alzheimerovou chorobou a deseti zdravých kontrol bylo měřeno množství traktů, délka traktů, objem traktů, kvantitativní anizotropie a generalizovaná frakční anizotropie. U pacientů s Alzheimerovou chorobou byl ve srovnání s kontrolami zjištěn významný pokles počtu traktů a generalizované frakční anizotropie v pravém nucleus caudatus, zatímco v levém a pravém putamen byl zjištěn nárůst. Dále byl pozorován významný pokles strukturálního objemu levého a pravého putamen. Zvýšení parametrů DTI bílé hmoty u pacientů s Alzheimerovou chorobou bylo pozorováno pouze v putamen oboustranně. Pravý nucleus caudatus vykazoval u pacientů s Alzheimerovou chorobou pokles jak parametrů DTI, tak objemu. Pravé pallidum vykazovalo u pacientů s Alzheimerovou chorobou zvýšení parametrů DTI, ale i snížení objemu.

Klíčová slova

Alzheimerova choroba, schizofrenie, morfometrie, FreeSurfer, ImageJ, sulcus cinguli, sulcus paracingularis, hipokampus, bazální ganglia, bílá hmota, šedá hmota, traktografie, atrofie, parcelace, mozková kůra

Abstract

Cortical folding of the anterior cingulate cortex (ACC), particularly the cingulate (CS) and the paracingulate (PCS) sulci, represents a neurodevelopmental marker. Deviations in in utero development in schizophrenia can be traced using CS and PCS morphometry. In the present study, we measured the length of CS, PCS, and their segments on T1 MRI scans in 93 patients with first episode schizophrenia and 42 healthy controls. Besides the length, the frequency and the left-right asymmetry of CS/PCS were compared in patients and controls. Distribution of the CS and PCS morphotypes in patients was

different from controls. Parcellated sulcal pattern CS3a in the left hemisphere was longer in patients (53.8 ± 25.7 mm vs. 32.7 ± 19.4 mm in controls, $p < 0.05$), while in CS3c it was reversed—longer in controls (52.5 ± 22.5 mm as opposed to 36.2 ± 12.9 mm, n.s. in patients). Non parcellated PCS in the right hemisphere were longer in patients compared to controls (19.4 ± 10.2 mm vs. 12.1 ± 12.4 mm, $p < 0.001$). Therefore, concurrent presence of PCS1 and CS1 in the left hemisphere and to some extent in the right hemisphere may be suggestive of a higher probability of schizophrenia.

Measurement of an hippocampal area or volume is useful in clinical practice as a supportive aid for diagnosis of Alzheimer's disease. Since it is time consuming and not simple, it is not being used very often. We present a simplified protocol for hippocampal atrophy evaluation based on a single optimal slice in Alzheimer's disease. We defined a single optimal slice for hippocampal measurement on brain magnetic resonance imaging (MRI) at the plane where the amygdala disappears and only the hippocampus is present. We compared an absolute area and volume of the hippocampus on this optimal slice between 40 patients with Alzheimer disease and 40 age-, education- and gender-matched elderly controls. Furthermore, we compared these results with those relative to the size of the brain or the skull: the area of the optimal slice normalized to the area of the brain at anterior commissure and the volume of the hippocampus normalized to the total intracranial volume. Hippocampal areas on the single optimal slice and hippocampal volumes on the left and right in the control group were significantly higher than those in the AD group. Normalized hippocampal areas and volumes on the left and right in the control group were significantly higher compared to the AD group. Absolute hippocampal areas and volumes did not significantly differ from corresponding normalized hippocampal areas as well as normalized hippocampal volumes using comparisons of areas under the receiver operating characteristic curves. The hippocampal area on the well-defined optimal slice of brain MRI can reliably substitute a complicated measurement of the hippocampal volume. Surprisingly, brain or skull normalization of these variables does not add any incremental differentiation between Alzheimer disease patients and controls or give better results.

The volume reduction of the gray matter structures in patients with Alzheimer's disease is often accompanied by an asymmetric increase in the number of white matter fibers located close to these structures. The present study aims to investigate the white matter structure changes in the motor basal ganglia in Alzheimer's disease patients compared to healthy controls using diffusion tensor imaging. The amounts of tracts, tract

length, tract volume, quantitative anisotropy, and general fractional anisotropy were measured in ten patients with Alzheimer's disease and ten healthy controls. A significant decrease in the number of tracts and general fractional anisotropy was found in patients with Alzheimer's disease compared to controls in the right caudate nucleus, while an increase was found in the left and the right putamen. Further, a significant decrease in the structural volume of the left and the right putamen was observed. An increase in the white matter diffusion tensor imaging parameters in patients with Alzheimer's disease was observed only in the putamen bilaterally. The right caudate showed a decrease in both the diffusion tensor imaging parameters and the volume in Alzheimer's disease patients. The right pallidum showed an increase in the diffusion tensor imaging parameters but a decrease in volume in Alzheimer's disease patients.

Keywords

Alzheimer's disease, schizophrenia, morphometry, FreeSurfer, ImageJ, sulcus cinguli, sulcus paracingularis, hippocampus, basal ganglia, white matter, gray matter, tractography, atrophy, parcellation, cortex

List of abbreviations

ACC - anterior cingulate cortex
AD - Alzheimer's disease
ADC - Alzheimer's disease continuum
AUC-ROC - area under the curve (receiver operating characteristic curve)
CA - commissura anterior
CC - corpus callosum
CNS - central nervous system
CS - sulcus cinguli
CSF - cerebrospinal fluid
dACC - dorsal anterior cingulate cortex
DSI - diffusion spectrum imaging
DTI - diffusion tensor imaging
DWI - diffusion weighted imaging

ESO - Early-Stage Schizophrenia Outcome study

FA - fractional anisotropy

FES - First-episode schizophrenia

GAM - generalized additive model

GFA - generalized fractional anisotropy

GQI - generalized Q-sampling imaging

MCI - mild cognitive impairment

MMSE - mini-mental state examination

MNI Space - Montreal Neurological Institute space

MRI - magnetic resonance imaging

NIA-AA - National Institute on Aging-Alzheimer's Association

NIMH - National Institute of Mental Health

nQA - normalized quantitative anisotropy

NT - number of tracts

ODF function - orientation distribution function

PC - personal computer

PCC - posterior cingulate cortex

PCS - sulcus paracingularis

PT - planum temporale

QA - quantitative anisotropy

QBI - q-ball imaging

QSDR - q-space diffeomorphic reconstruction

ROC - receiver operating characteristic curve

rWTH - radial width of the temporal horn

SDF - spin distribution functions

TIV - total intracranial volume

vACC - ventral anterior cingulate cortex

WM - white matter

Content

1. Introduction

1.1 Anatomical changes in the brain structure in Alzheimer's disease and schizophrenia

Alzheimer's disease and schizophrenia are two distinct disorders that are associated with different anatomical changes in the brain structure.

Alzheimer's disease is a progressive neurodegenerative disorder that primarily affects the memory and cognitive functions of the brain (Tang et al., 2019). The main anatomical changes in the brain structure in Alzheimer's disease are the accumulation of beta-amyloid plaques and neurofibrillary tangles, which derange the normal communication between neurons and cause neuronal death (Perl, 2010). These changes primarily take place in the hippocampus (Lakshmisha Rao et al., 2022) and temporal lobes of the brain, which are crucial for memory formation and reconsolidation. As the disease progresses, the changes may spread to other parts of the brain, leading to widespread neurodegeneration and cognitive decline. A study has revealed that patients with Alzheimer's disease indicate depletion in the thickness of layer III pyramidal neurons in specific regions of the brain. The affected regions incorporate the right anterior cingulate gyrus, the left posterior cingulate gyrus, and entorhinal cortex, and the right parahippocampal gyrus (Kutová et al., 2018) that are parts of the limbic system.

Schizophrenia, otherwise, is a serious mental disorder identified by disarranging in thoughts, emotions, and behavior (McGrath et al., 2008). The morphological alterations in the brain structure in schizophrenia are more implicit than those in Alzheimer's disease, but they are still consequential (Shenton et al., 2010). Research established that patients with

schizophrenia have reduced gray matter volume in some areas of the brain, including the prefrontal cortex, temporal lobe, and hippocampus (van Erp et al., 2016). Furthermore, there is confirmation of changes in connectivity between distinct regions of the brain in schizophrenia, which may grant to the cognitive and behavioral symptoms of the disorder. Several studies showed that the areas presenting the most remarkable decline in connectivity include the medial prefrontal cortex, anterior and posterior cingulate, temporal lobe, lobule IX of the cerebellum, and premotor cortex (Orban et al., 2019).

1.2 History of neuromorphometry

Neuro morphometry is the quantitative analysis of the morphology of neurons and other structures in the nervous system using computer-based imaging techniques (Haug, 1986). It originates in the end of the 19th century when scientists started to research the three-dimensional structures of neurons and other cells using light and electron microscopy (Guillery, 2005). It was the work of Spanish neuroscientist and pathologist Santiago Ramón y Cajal (1899) who was awarded the Nobel Prize in Physiology or Medicine in 1906, which he shared with the Italian physician Camillo Golgi. The Nobel Committee mentioned Cajal's work in proceeding our understanding of the "fine structure of the nervous system" (de Castro, 2019). Cajal's finding of separate neurons and their extensions like dendrites and axons, helped to create the cell doctrine of the nervous system (Guillery, 2005).

One of the first innovations in the field of neuro morphometry emerged in the 1960s when scientists started to use stereological methods to evaluate the entire quantity of neurons in diverse brain regions (Cruz-Orive, 2017). Biologist Hans Elias created the definition of 'stereology' as a method for obtaining 3D information from 2D images (Elias, 1963). This technique empowers researchers to measure quantitative characteristics of neuronal density and different morphological landmarks of the brain (Maina, 2017).

Development of advanced computer technologies and digital image processing led to the appearance of more sophisticated techniques for analyzing and quantifying neuronal morphology, such as the novel Sholl analysis to measure dendritic branching and complexity, and the dendritic spine analysis, which quantifies the number and shape of spines on the dendrites (Langhammer et al., 2010).

Nowadays neuro morphometry keeps up to be a principal tool for studying the anatomy of the brain and for understanding how altered neuro morphology contributes to neurological and psychiatric disorders. It is used in both basic research and clinical settings and has the potential to help develop new treatments for a variety of brain disorders.

1.3 A structural MRI studies of the brain

Magnetic resonance imaging is a technology that uses radio frequency signals from hydrogen protons in the body to form images of body structure (Berger, 2002). MRI works on special magnets that create a strong magnetic field that directs the protons in the body according to this field. When a radiofrequency current is passed through the patient, the protons are stimulated and out of equilibrium. As soon as the radiofrequency field is stopped, the MRI sensors could confirm the energy released as the protons realign with the magnetic field (Orth, 2012). There are two relaxation times associated with proton rearrangement: T1 and T2. T1-weighted MRI elevates adipose tissue signal and declines water signal. T2-weighted MRI increases the water signal (Kawahara et al., 2021). Both images have excellent soft tissue contrast.

The first MRI studies of the brain concentrated on creating techniques to acquire high-resolution images of the brain's internal structures, such as the gray and white matter, ventricles, and blood vessels (Jahng et al., 2020). Scientists also worked to develop methods for distinguishing between normal and abnormal brain tissue, such as tumors and regions of inflammation (Horská et al., 2010).

Years since its appearance, MRI has become the gold standard for imaging the brain, presenting higher-ranking resolution and contrast compared to other methods (Chandarana et al., 2018). It has enabled researchers and clinicians to make important discoveries about the structure and function of the brain, as well as to diagnose and treat a wide range of neurological conditions, including stroke, multiple sclerosis, schizophrenia and Alzheimer's disease.

1.4 MRI and hippocampal volume reduction in AD

Several research studies have documented a reduction in hippocampal volume among individuals with Alzheimer's disease (AD) in comparison to elderly controls (Shi et al., 2009). In the Alzheimer's disease continuum (ADC), neurodegeneration initiates in the transentorhinal cortex and advances through the hippocampal circuitry, following the transsynaptic connectivity of its subfields (Hari et al., 2022).

This change leads to the strong cognitive impairment for patients connected with the hippocampal texture marker correlated with hippocampal glucose metabolism, as suggested by fluorodeoxyglucose-positron emission tomography (Sørensen et al., 2016).

1.5 Asymmetry of the structural changes of the gray and white matter in the CNS in AD

Observations of brain asymmetry in norm have been made in both animals and humans, spanning across structural, functional, and behavioral domains (Geschwind, 1965). This lateralization is believed to represent a range of influences, including evolutionary, hereditary, developmental, experiential, and pathological factors, because the left and right hemispheres of the brain have differential growth patterns and connectivity that was already proven from various imaging techniques, such as magnetic resonance imaging (MRI) and diffusion tensor imaging (DTI), which have allowed for the examination of the asymmetries in gray and white matter in vivo (Good et al., 2001).

One example of structural asymmetry in gray matter is the planum temporale in the temporal lobe, which is consistently larger in the left hemisphere in most individuals. This region is important for language processing and has been implicated in speech perception and phonological processing. In contrast, the right hemisphere appears to have a greater volume of gray matter in the superior parietal lobule, which is involved in spatial processing and attention (Toga et al., 2003). Asymmetric changes in the size and number of neurons in the limbic cortex and planum temporale were found in AD patients compared to controls (Kutova et al., 2018). The overall planum temporale right and left size differed in AD patients and also in schizophrenia (Zach et al., 2009), as did the size of pyramidal neurons in different subdivisions of the planum temporale in AD patients (Kutova et al., 2014). In an animal study of the effect of chronic stress on hippocampal area and volume, a

more pronounced atrophy of the right hippocampus compared to the left was found, although the exact reason is still unclear (Zach et al., 2010).

Previous findings of asymmetric morphology of CNS structures is important for our studies, in which (see Results) we also observed such asymmetric impairment (or adaptation).

1.6 Neuroanatomy of anterior cingulate cortex and its clinical significance

The anterior cingulate cortex (ACC) lies on the medial surface of the brain and is composed of several subregions. Two of them, the cingulate sulcus (CS) and the paracingulate sulcus (PCS) might play an important role in relation to schizophrenia.
The CS runs along the callosal body and extends posteriorly into the parietal lobe as the marginal branch. From the dorsal to the anterior portion of the CS, a sulcus that is often present and runs parallel to the CS is referred to as the paracingulate sulcus (Smith, 1907). The PCS shows significant individual and hemispheric differences. While the CS is present in the majority of cases, the PCS is frequently missing or rudimentary (Wei et al., 2017). Although it was recently reported to be present in 70.1% of the human population (Amiez et al., 2021). Leftward asymmetry of PCS has been reported in healthy controls (Wei et al., 2017; Yücel et al., 2001; Paus et al., 1996). Inter-individual variation in the PCS presence is transposed into the prenatal formation of single or double parallel type of the ACC, which is reported in 76% and 24% of adults, respectively (Ono et al., 1990).

From the developmental perspective, the first appearance of the CS was reported in the 19th week of the fetal period, and the marginal branch of the CS at the 30th ± 3 weeks (Nishikuni et al., 2013). An ultrasound study in 677 term-born neonates clearly identified four distinct major folding patterns in the CS (Meng at al., 2018) which is consistent with reports of the adult brain folding patterns on the MRI and autopsy materials (Sun et al., 2009). Subsequently, an individual ACC sulcal pattern remains fixed from childhood to adulthood, at the same time that quantitative structural ACC metrics are undergoing profound developmental change (Cachia et al., 2016).

Empirical evidence for the neurodevelopmental and/or neurodegeneration origin of schizophrenia is still a matter of debate (Weinberger et al., 2003; Woods et al., 1998). Abnormalities in the anterior cingulate cortex (ACC) region proven by structural magnetic resonance imaging (MRI) accompanied by neuropathological findings and working

memory processing deficit (Feng et al., 2023) may testify to a neurobiological basis for schizophrenia (Fornito et al., 2008). Brugger and Howes in their meta-analysis from 2017 based on MRI morphometry from 3901 patients with first-episode schizophrenia and 4040 controls discovered greater homogeneity of the ACC volume and significantly lower mean volume, which may signalize schizophrenia (Brugger et al., 2017). Modified controllability of functional activity in dorsal ACC may also play an important role in the pathophysiology of schizophrenia, consistent with the importance of this region in cognitive and brain state control operations (Li et al., 2023). At the same time, available findings point to the fact that the ACC gray matter reductions precede psychosis onset and that neurodevelopment of the ACC region might thus be in play (Fornito et al., 2009).

All of the above underlines the importance of quantification of the ACC folding pattern in schizophrenia. Assessment of sulcal patterning in the ACC may serve as a macroscopic probe for hidden developmental events within this area.

1.7 Problem in establishing the optimal section for the hippocampus and its clinical significance

The hippocampus is a region of the brain that plays an important role in learning, memory, and spatial navigation. It is located in the medial temporal lobe, which is situated in the center of the brain. The exact positioning of the hippocampus within the brain is crucial for understanding its functions and for performing surgical interventions.

One problem in establishing the optimal section for the hippocampus is that it varies in size and shape between individuals. In addition, the hippocampus is surrounded by other structures that can make it difficult to identify and access during surgery.

Another important consideration in positioning the hippocampus is its functional connectivity with other areas of the brain. The hippocampus is known to be involved in a variety of cognitive processes, including memory, spatial navigation, and emotion regulation. Therefore, it is important to consider the potential impact of surgical interventions on these functions and to take steps to minimize any negative effects.

Measurement of an- hippocampal area or volume is useful in clinical practice as a supportive aid for diagnosis of Alzheimer's disease. Since it is time-consuming and not simple, it is not being used very often. At the same time rating of medial temporal lobe atrophy is recommended in all current diagnostic guidelines to diagnose dementia (Harper

et al., 2015). Total brain volume and volume-to-brain ratio in comparison to hippocampal and temporal horn measurements in traumatic brain injury showed hippocampal atrophy and temporal horn enlargement. The hippocampus and temporal horn volumes were inversely correlated in the group with traumatic brain injury (Bigler et al., 1997). The inverse relationship between the hippocampus and adjacent ventricle or the third ventricle is also used for detection of Alzheimer's disease (Bartoš et al., 2019; Schoemaker et al., 2019). The measure of temporal atrophy (radial width of the temporal horn (rWTH)) was used to distinguish its asymmetry in AD patients (Geroldi et al., 2000). Anatomical mapping of structural changes in AD showed more sensitive temporal horn expansion compared to hippocampal atrophy, but both maps correlated with clinical findings (Thompson et al., 2004).

1.8 Concept of compensatory hypertrophy of white matter surrounding structures of the basal forebrain in AD or other neurodegenerative diseases

The concept of adaptive white matter changes in neurodegenerative diseases is relatively new (Tuladhar et al., 2015; Zhang et al., 2023; Grady et al., 2003). It is based on the assumption that atrophy of parts of the white matter, such as in Alzheimer's disease patients, results in reactive hypertrophy (functional or morphological) in adjacent or even remote parts of the brain, which would then be able to take over the function of the damaged part to some extent. In our studies, we have described such changes in the area subcallosa and gyrus paraterminalis, as well as in some basal ganglia (putamen, pallidum and caudate).

Our finding of white matter increase in the area subcallosa and gyrus paraterminalis was the basis for a human study to demonstrate improved memory performance in Alzheimer's disease patients as a consequence of morphological and functional compensatory white matter hypertrophy (published in the prestigious NEJM, Deeb et al., 2019). Briefly, when the fornix and other parts of the CNS were stimulated with ascending voltages (7-10 V) in vivo by applied electrodes, Alzheimer's disease patients showed a significant recovery from memory of an event that had been completed by the participants prior to the experiment. The maximum retrieval of episodic events was maintained when a voltage of 10 V was applied.

2. Hypothesis and goals

2.1 Particular subtype of CS and PCS cortex morphology could be specific for patients with schizophrenia (study no. 1)

Numerous studies in the literature document the relationship between the morphological changes of the central nervous system and schizophrenia, e.g., cortical areas (Vita et al., 1988), amygdala (Mahon et al., 2012), hippocampus (Heckers, 2001), and others (Breier et al., 1992), but they are not suitable for morphological diagnosis of schizophrenia because of their non-specificity and frequent anatomical variability. The CS and the PCS are two regions found within the ACC on the medial side of the brain hemisphere. Morphological variability of the PCS was described, for example, in (Garrison et al., 2015). Specificity of the morphological changes in ACC vs. other cortical areas were described by (Fornito et al., 2009). Variability in the CS organization in human adult and fetal cadavers was described by (Marinescu et al., 2018). The CS structure was analyzed in six groups of adult brains whose medial hemisphere was parcellated into I-III sectors, clockwise to the CS course. The major differences in the CS organization could be summarized into the following observations: in sector I the subgenual part of callosal body varies in the numbers and shape of the CS infoldings; in sector II there is broken trajectory of the CS by the dorsal cingulate-frontal infolding; and in sector III the trajectory is sinusoid and there is a convoluted aspect of the marginal branch. It is still difficult to account for these variations on the MRI where tiny details of the CS neuroanatomy are often blurred by the arachnoid.

2.2 In patients with schizophrenia marked asymmetry of CS and PCS compared to controls (study no. 1)

Our hypothesis was that more pronounced changes in CS and PCS length and parcellation would be located in the right cerebral hemisphere. This assumption is based on

the introduction of the cited papers, where similarly larger changes in the planum temporale or hippocampus are also observed on the right.

2.3 Possibility of selecting 'optimal frontal section' of the hippocampus so it could be used for the visual assessment of the hippocampal atrophy in patients with Alzheimer disease (study no. 2)

Our hypothesis was that it is possible to select an optimal coronal MRI slice from which to determine hippocampal atrophy in AD patients in the office by simply inspecting the image. This involved finding the site of the hippocampal size transition where the ratio of the size of the cornu temporale to the lateral ventricle is clearly visible over the widest area of the coronal section of the hippocampus. Such a procedure would facilitate the time-consuming reconstructions and volumetrics of the hippocampus performed using reconstruction software on computers and would facilitate the diagnosis of visual atrophy of the hippocampus in AD.

2.4 Compensatory changes in BG - hypertrophy of gray matter or surrounding white matter following progression of atrophy in other structures in patients with Alzheimer's disease (study no. 3)

Based on a previous study by (Kuchtová et al., 2018) where compensatory hypertrophy of the area subcallosa and gyrus paraterminalis was observed in AD patients, probably as a consequence of atrophy and altered hippocampal function, we hypothesized that a similar phenomenon may occur in the basal ganglia. Thus, again, compensatory hypertrophy of either the basal ganglia themselves or the white matter in their immediate surroundings, as an expression of increased functional connectivity, particularly with cortical areas.

2.5 All the above mentioned hypotheses are supplemented with asymmetry assessment, so that our prediction would be right side dominance over the left one (studies no.1-3)

In all of the above hypotheses, we hypothesized (see study no. 1) that the observed changes would be more pronounced in the right hemisphere. Specifically, that the CS and PCS would be shorter and more segmented on the right in schizophrenia patients, that the optimal hippocampal section would be smaller on the right in both AD patients and controls, and finally that the increase in the volume of the BG (one or more of them) and/or the white matter hypertrophy in their surroundings would also be more pronounced on the right.

3. Overview of used methods and techniques

Structural imaging methods such as MRI was the main one used during that study. Routine MR images were analyzed through FreeSurfer (v6.0) and FiJi (ImageJ) software, while diffusion tensor images (DTI) were analyzed through the FSL Studio program. Statistics were performed through Statistica v.6., v.10., v.13 software, online Effect Size Calculator, MedCalc v. 19.2.1, R environment. The Mini-Mental State Examination (MMSE) scale is used to detect mild cognitive impairment (MCI) in Alzheimer's disease patients. Clinical information about Early-Stage Schizophrenia Outcome study (ESO) for the first episode schizophrenia (FES) patients received from the National Institute of Mental Health, Klecany, Czech Republic (NIMH).

3.1 Schizophrenia patients and control group

A total of 93 patients with a first episode of schizophrenia (FES, patients) and 42 healthy participants (controls) were recruited (Table 1). The sample of patients came from the Early-Stage Schizophrenia Outcome study (ESO), a prospective study on subjects with FES conducted at the National Institute of Mental Health, Klecany, Czech Republic (NIMH). Patients with FES were recruited between 2015 and 2019 through the ESO

recruitment network, which includes five large psychiatric hospitals in the country (total of 3700 beds), with a total catchment area of 6.5 million people. The criteria for inclusion in the FES were as follows: (1) a diagnosis of schizophrenia or schizophreniform illness or a diagnosis of acute polymorphic psychotic disorder made by a psychiatrist in accordance with the Psychiatric Care Act according to the criteria of the International Classification of Diseases-10; (2) a first episode of psychotic illness diagnosed according to the criteria of the International Classification of Diseases-10; and (3) a duration of untreated psychosis of less than 24 months. All patients with a psychotic mood disorder (including schizoaffective disorder, bipolar disorder, and unipolar depression with psychotic symptoms) were excluded from the study (Table 2). All patients The ESO was approved by the NIMH Ethics Committee. The study was conducted in accordance with the latest version of the Declaration of Helsinki.

Table 1. Demographic data of schizophrenia patients and healthy controls. The data are presented as mean values ± SD.

	Patients sample total (n = 93)	Healthy controls (n = 42)
Sex, n = male/female	47/46	17/25
Age at baseline MRI (V1), year	30.1 ± 7.4	31.6 ± 6.2
Age at second, follow up MRI (V2), year	31.3 ± 7.4	32.6 ± 5.6
Years of education at V2	14.8 ± 3.1*	17.9 ± 3.6*
Interscan interval (V1-V2), month	13.0 ± 1.8	16.0 ± 3.8

Table 2. Characteristics of the patients and diagnoses. The data are presented as mean values ± SD.

Detailed overview of patient´s examination	
Age at onset, year	29.4 ± 7.3
Duration of illness (DUI) at baseline V1, month	7.7 ± 11.2
Duration of untreated psychosis (DUP), month	4 ± 11.9
Global Assessment of Functioning (GAF) at V1	65.6 ± 15.4
Global Assessment of Functioning (GAF) at V2	79.9 ± 13.0
Positive and Negative Syndrome Scale (PANSS) negative 1	15.7 ± 5.8
Positive and Negative Syndrome Scale (PANSS) negative 2	13.3 ± 5.4
Positive and Negative Syndrome Scale (PANSS) 1Σ	60 ± 16.0
Positive and Negative Syndrome Scale (PANSS) 2Σ	48.2 ± 14.6

Final diagnosis (M/F)	
Schizophrenia	29/30
Acute polymorphic psychotic disorder without symptoms of schizophrenia	3/2
Acute polymorphic psychotic disorder with symptoms of schizophrenia	9/11
Acute schizophrenia-like psychotic disorder	2/0
Other acute predominantly delusional psychotic disorders	1/0
Schizoaffective disorder	1/5

3.2 Image J program and cingulate cortex morphology in patients with schizophrenia

To measure the size of the sulcus cinguli and sulcus paracingularis, Image J (FiJi, Linux version, https://imagej.net/software/fiji/downloads) and MRIcron (https://www.nitrc.org/projects/mricron) were installed in the XnView environment. The MRIcron program was used to transpose the MRI images to all three planes (sagittal, frontal and horizontal). To verify the setup, the MRI planes were then set up and compared directly in Image J (reslice option). The transformed files were saved in the Analysis and Data directory to avoid increasing the data volume on the work server.

The length of the sulcus cinguli and sulcus paracingularis was determined in multiple sagittal planes on MRI images. The reasons for measuring multiple sagittal planes were the curvature of the cerebral hemispheres, differences in brain rotation during MRI scanning, and differences in the depth of the sulci between the gyri or their irregular discontinuity during the course. Thus, the patterns of all sulci variants were evaluated. The set scale for each brain was set in Image J automatically, from the MRI image table.

3.3 Detailed neuroanatomy of the CS and PCS patterns in patients with schizophrenia

Generally, the CS is always present in the brain while the PCS may not be present at all. The CS is located on the medial part of both the left and right hemispheres. In its major course, it separates the cingulate gyrus from the gyri located above. It often starts in the frontal lobe at the level of the anterior cingulate gyrus and continues dorsally upward between the paracentral lobule and the praecuneus. The PCS, if present, is located above the CS, usually at the level of the ventral portion of the anterior cingulate gyrus (Wei et al.,

2017). Manual delineation of any brain structure requires advanced morphological and topographical expertise for precise delineation of the structures of interest. The CS starts in the subcallosal area and has an arched course, running above the cingulate gyrus. This way it separates the medial frontal and the parietal cortices from the limbic structure — the cingulate gyrus. Gross delineation of the cingulate sulcus on the MRI is associated with the cingulate gyrus, especially its anterior and posterior portions. The posterior cingulate gyrus is bordered by the marginal ramus of the cingulate sulcus (above), the callosal body (caudally), the parieto-occipital sulcus (dorsally), and the Brodmann area 24 (ventrally). This corresponds to the transition between the anterior and posterior cingulate gyri. Near the connection between the isthmus of the cingulate gyrus and splenium of the corpus callosum, the marginal branch of the cingulate sulcus reaches the superior end of the hemisphere (Destrieux et al., 2017). According to Terminologia Neuroanatomica (FIPAT, 2017), we did delineation of the ventral and dorsal borders of the CS in the Cartesian coordinate plane with the center at the level of Monro's interventricular foramen. We characterized borders in accordance with the following anatomical regions: the ventral anterior cingulate cortex (vACC), the dorsal anterior cingulate cortex (dACC), and the posterior cingulate cortex (PCC). The CS arises as a profound groove in the vACC, from under the genu of callosal body and the rostral gyrus and then it runs parallel to the upper frontal gyrus (Figure 1). The trajectory of the CS is interrupted in the dACC by the dorsal cingulate-frontal infolding. In the PCC, after a horizontal trajectory parallel to the body of the callosal body, CS is interrupted again by the anterior cingulate-parietal connective infolding (Marinescu et al., 2018).

First, we measured non-parcellated CS and PCS (without separation of the sulci course into interrupted segments). Next, we performed the segmentation of the CS and PCS. We measured the linear length of the CS and observed how many parts it was composed of in the case of interruption — in other words, CS morphology was assessed depending on the integrity of the sulcal line. If there was no interruption of the sulcus, we labeled it as CS1, one interruption of the sulcus was labeled as CS2, and two interruptions were labeled as CS3. For the length measurement, two sulcal parts (segments) of CS2 were labeled as CS2a and CS2b, and three sulcal parts of CS3 were labeled as CS3a, CS3b, and CS3c, and their length was measured separately (Table 3). Indexing parts (segments) followed the ventro-dorsal position so that, for example, CS2a was located more ventrally compared to CS2b. The neuroanatomical delineation of the PCS was adapted according to J. R. Garrison's Paracingulate Sulcus Measurement Protocol (Garrison, 2017), based on

the original study (Garrison et al., 2015). We selected the PCS sulcal pattern parcellation identical with Yücel's nomenclature (three sulcal patterns type — absent, present, and prominent), (Yücel et al., 2001). PCS morphology was assessed as absent if the length was less than 2 cm (PCS0), present if it extended more than 2 cm (PCS1), and prominent if it was longer than 4 cm (PCS2), (Figure 2).

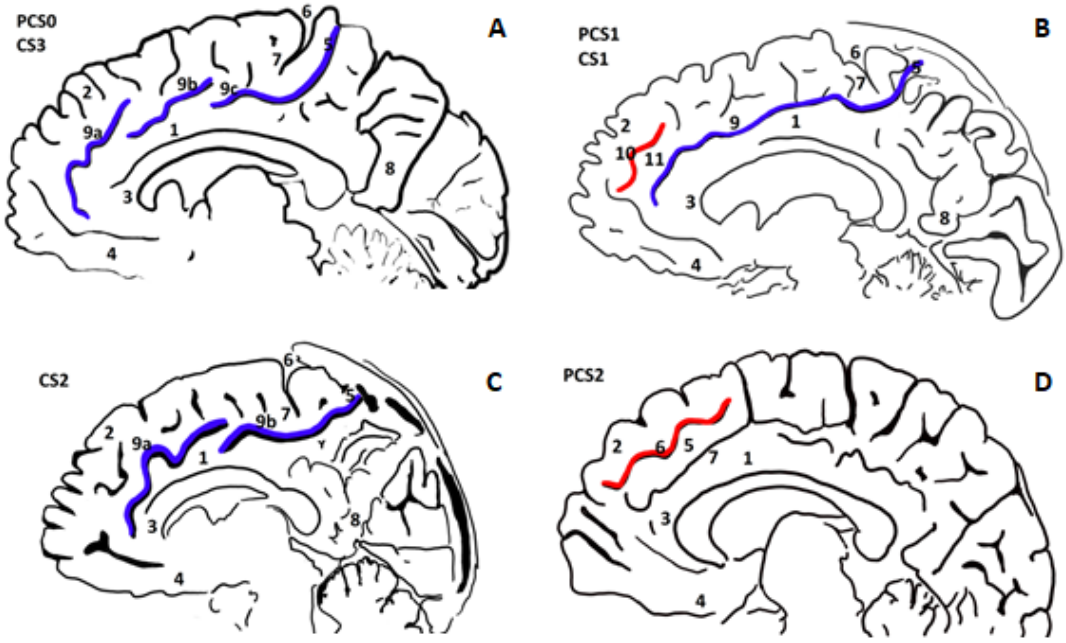

Figure 1. CS and PCS delineations on the medial hemisphere (right) of the brain. Combinations PCS0 and CS3, PCS1 and CS1, PCS2 alone, and CS2 alone do not reflect their co-occurrence in the patients; ether they were clustered together for better illustration. PCS0 means there is no paracingulate sulcus or its length is shorter than 2 cm.
Legend:

A) PCS0 and CS3: 1 – cingulate sulcus, 2 – superior frontal gyrus, 3 – genu corporis callosi, 4 – gyrus rectus, 5 – the marginal branch of cingulate sulcus, 6 – central sulcus, 7 – paracentral lobule, 8 – precuneus gyrus, 9a – cingulate sulcus (part one, CS3a), 9b – cingulate sulcus (part two, CS3b) and 9c – cingulate sulcus (part three, CS3c).
B) PCS1 and CS1: 1 – cingulate sulcus, 2 – superior frontal gyrus, 3 – genu corporis callosi, 4 – gyrus rectus, 5 – the marginal branch of cingulate sulcus, 6 – central sulcus, 7 – paracentral lobule, 8 – precuneus gyrus, 9 – cingulate sulcus (without interruption, CS1), 10 – paracingulate sulcus, 11 – paracingulate gyrus (without interruption, PCS1).
C) CS2: 1 – cingulate sulcus, 2 – superior frontal gyrus, 3 – genu corporis callosi, 4 – gyrus rectus, 5 – the marginal branch of cingulate sulcus, 6 – central sulcus, 7 – paracentral lobule, 8 – precuneus gyrus, 9a – cingulate sulcus (part one, CS2a), 9b – cingulate sulcus (part two, CS2b).

D) PCS2: 1 – cingulate sulcus, 2 – superior frontal gyrus, 3 – genu corporis callosi, 4 – gyrus rectus, 5 – paracingulate gyrus, 6 – paracingulate sulcus, 7 – cingulate sulcus.

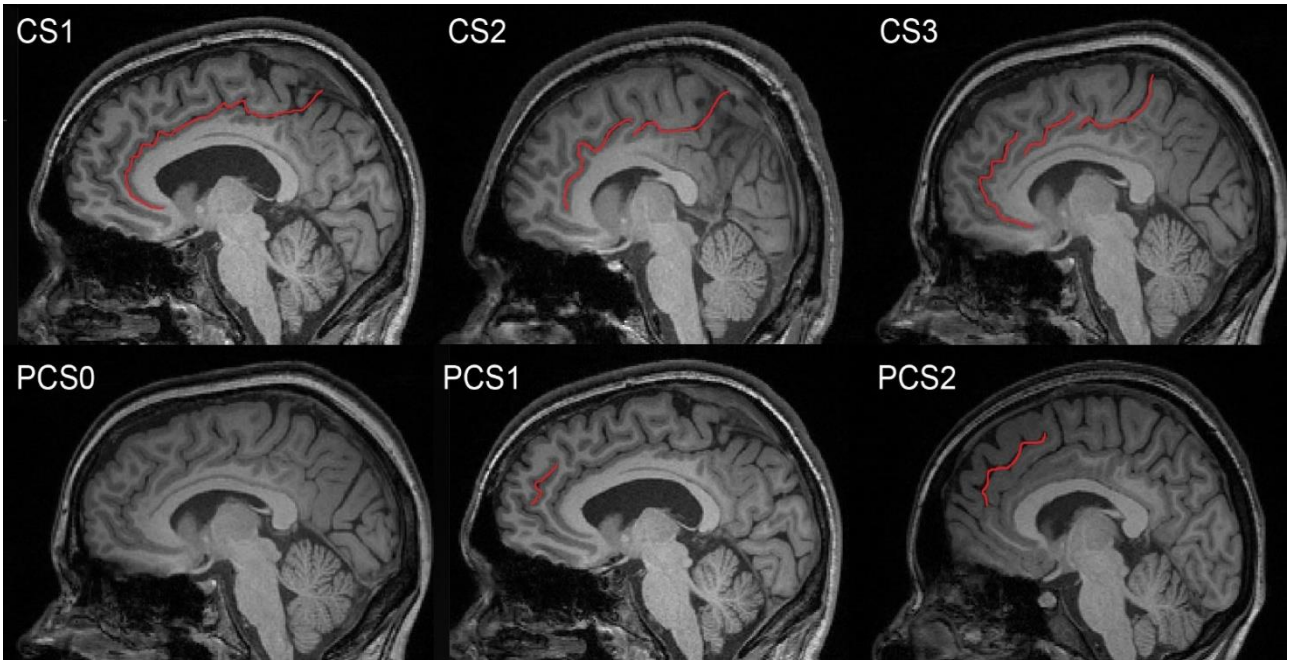

Figure 2. Illustrative examples of possible appearances of CS and PCS morphology types on the MRI images.

Table 3. Detailed analysis of the length of the parcellated CS and PCS on the left and right side in schizophrenia patients and controls and their incidences. The data are presented for all types of morphology (CS types 1, 2, 3 and PCS types 0, 1, 2). The length data are presented as mean values in mm ± SD. The incidence is presented as a number of cases (n) and their percentages. Incidences of CS types 2 and 3 are given as a single value for all relevant sulcal parts (segments). Statistical significance was calculated by non parametric Mann - Whitney U test and Kruskal-Wallis test ($p<0.05$ and $p<0.001$).

Brain structures	Patients		Controls	
	length in mm	incidence in (%)	length in mm	incidence in (%)
Left cingulate sulcus type 1 (CS1)	110.7 ± 15.8	61 (66)	105.2 ± 21.7	6 (14)

Left cingulate sulcus type 2a (CS2a)	59.8 ± 16.3	26 (28)	52 ± 19.3	17 (41)
Left cingulate sulcus type 2b (CS2b)	55.9 ± 18.3		62.9 ± 26	
Left cingulate sulcus type 3a (CS3a)	53.8 ± 25.7 p<0.05	6 (6)	32.7 ± 19.4 p<0.05	19 (45)
Left cingulate sulcus type 3b (CS3b)	20.5 ± 9		22.3 ± 12.9	
Left cingulate sulcus type 3c (CS3c)	36.2 ± 12.9		52.5 ± 22.5	
Right cingulate sulcus type 1 (CS1)	113.3 ± 18.7	58 (63)	123.2 ± 19.1	5 (12)
Right cingulate sulcus type 2a (CS2a)	65.9 ± 23.8	30 (32)	57.2 ± 26.7	18 (43)
Right cingulate sulcus type 2b (CS2b)	53.6 ± 2.3		63.8 ± 27.5	
Right cingulate sulcus type 3a (CS3a)	47.7 ± 7.7	5 (5)	35.9 ± 16.1	19 (45)
Right cingulate sulcus type 3b (CS3b)	39.2 ± 17.2		24.9 ± 19.7	
Right cingulate sulcus type 3c (CS3c)	34.5 ± 16.3		49.3 ± 20.1	
Left paracingulate sulcus type 0 (PCS0)	10.8 ± 4.8	63 (68)	10.9 ± 4.3	34 (81)
Left paracingulate sulcus type 1 (PCS1)	27.1 ± 4.7	30 (32)	29.3 ± 6.5	8 (19)
Left paracingulate sulcus type 2 (PCS2)	N/A	0 (0)	N/A	0 (0)
Right paracingulate sulcus type 0 (PCS0)	11.7 ± 5.2 p<0.001	51 (55)	6.2 ± 6 p<0.001	32 (76)

Right paracingulate sulcus type 1 (PSC1)	28.4 ± 5.2	41 (44)	28.2 ± 6.3	8 (19)
Right paracingulate sulcus type 2 (PCS2)	47.7 ± N/A	1 (1)	41.6 ± 2	2 (5)

3.4 Alzheimer's disease patients and control group

Brain magnetic resonance imaging (MRI) and the Mini-Mental State Examination (MMSE) were examined in 80 individuals during our validation and normative study of the MMSE. We included two groups of participants. The first group of patients (n = 40) was diagnosed with dementia due to Alzheimer's disease (AD) according to the National Institute on Aging-Alzheimer's Association (NIA-AA) criteria at memory clinic of the AD center, Department of Neurology, Charles University, Prague, Czech Republic. The second group of normal elderly controls (n = 40) had normal MMSE scores using our Czech norms and cut-offs for mild AD. They were recruited mainly at Universities of Third Age (educational courses for seniors) or were spouses of the patients. Sociodemographic characteristics and cognitive scores of both groups were compared (Table 4). All participants signed informed consent. The research was approved by the Ethics Committee of the Prague Psychiatric Center/National Institute of Mental Health.

Table 4. Characteristics of participants and group comparisons

	AD group	control group	p values
Numbers of participants	40	40	
Age at scan (years)	70.3 ± 6.8	67.8 ± 4.7	n.s
Education (years)	13 ± 3	14 ± 3	n.s
Male/female sex	13 / 27	15 / 25	n.s
MMSE score (0-30 pts.)	21 ± 1	29 ± 4	< 0.001

Data are expressed as mean ± standard deviation. MMSE − the Mini-Mental State Examination, n.s. – not significant.

3.5 Manual delineation of the hippocampal optimal section with Image J program

In order to define hippocampal shrinkage on MRI for the clinical applications (dementia severity and its progression), we designed a protocol from a single coronal brain slice. We found gray matter located inside the temporal lobe (at the caudal part of the temporal horn of the lateral ventricle) by viewing the coronal slice on MRI in ventrodorsal orientation (Figure 3). Then, we located the amygdalar complex in the temporal lobe, below the lateral horn of the lateral ventricle. When we looked through coronal slices located more dorsally, we could see the hippocampus positioned below the amygdalar complex. With the increase in coronal slice numbers, we could see alveus in the caudal and lateral part of the hippocampus. Fimbria hippocampi was located on the top surrounded by several amygdalar nuclei. We considered the optimal coronal slice where amygdalar nuclei were no longer visible (at the level of fimbria hippocampi) so that we could observe the full extent of the hippocampus: alveus, dentate gyrus, and fimbria fornicis, located on the parahippocampal gyrus (Figure 4). In case of hippocampal atrophy, there was a significant reduction of both the gray and the white matter so that fissura hippocampi became clearly visible horizontally at the transition between the hippocampus and subiculum (part of parahippocampal gyrus).

The absolute area of the hippocampus in cm^2 separately for the left and right sides from a single optimal slice and absolute area of the brain and skull slice in the coronal section at the level of commissura anterior (CA) were manually delineated and calculated by an experienced neuroanatomist using FiJi (ImageJ software suite, https://imagej.net/Fiji).

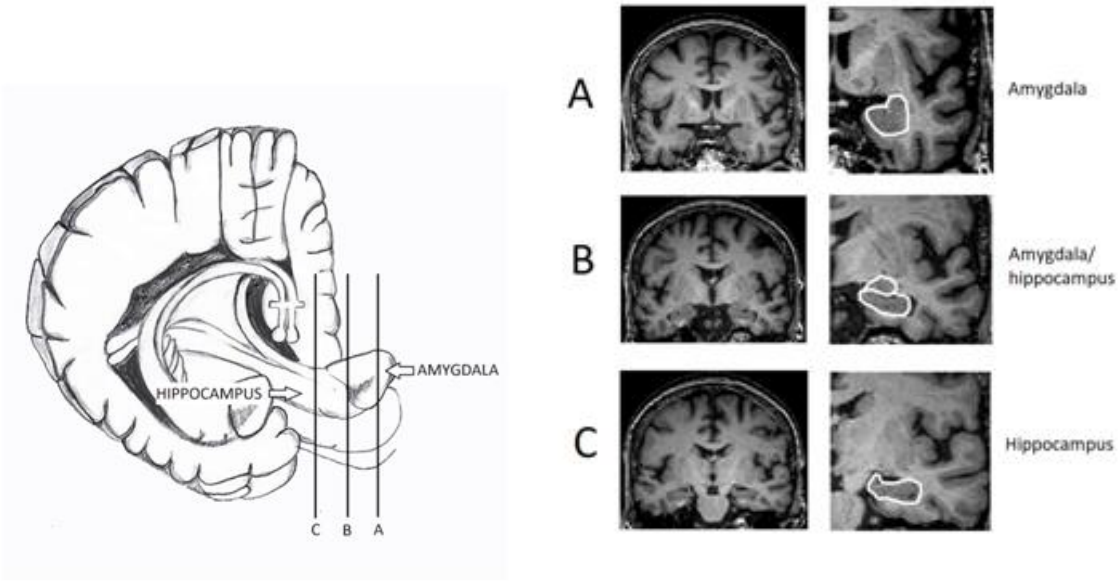

Figure 3. Procedure showing how to choose coronal **optimal slice** for hippocampal area measurement. The left figure shows brain structures involving the hippocampus and amygdala. There are three sections through different parts of these structures. They are labelled A, B, and C which correspond to the right magnetic resonance imaging slices in the left MRI column: A – slice through amygdala, B – slice through amygdala and hippocampus and C – slice only through hippocampus, or **optimal slice**. Detailed views of structures of interest are displayed in the MRI right column.

Figure 4. A detailed view of left mediotemporal structures on the **optimal slice** of brain MRI. Anatomical structures are labeled as follows: 1 - hippocampal fimbria, 2 - alveus, 3 - parahippocampal gyrus, 4 - subiculum, 5 - hippocampal fissure, 6 - uncus of the parahippocampal gyrus

3.6 Optimal slice of the hippocampus measurement and BG volumes in patients with Alzheimer's disease and controls by FreeSurfer analysis

For detailed familiarization with the FreeSurfer program, it was installed in the DOSBox version (Oracle Virtual Box 6.1.44 for Windows), (https://www.virtualbox.org/wiki/Download_Old_Builds_6_1) and as a training, reconstructions and analyses of MRI images of 5 controls were performed on local standard PCs at the Department of Anatomy. To analyze a statistically sufficient number of controls and patients with Alzheimer's disease, FS reconstructions and analyses of white and gray matter were performed on standard PCs at the National Institute of Mental Health in Klecany. All reconstructions were then entered into the MRAD database (database of images of controls and patients with Alzheimer's disease, AD Centrum Praha, FNKV, Prague 10). FS reconstructions were used to obtain automatic segmentation of white and gray matter, and then to determine TIV (total intracranial volume) for the possibility of normalizing the volume, area and size of hippocampal or basal ganglia structures in relation to the size of the brain in individual patients.

In the case of optimal slice, hippocampal areas were measured manually using Image J, but were normalized to TIV (cranial volume), which, together with hippocampal volumes, was measured automatically using the FreeSurfer program. Similarly, basal ganglia volumes were measured and calculated automatically using the FreeSurfer program.

3.7 DWI tractography and changes in the white matter around BG in patients with Alzheimer's disease

In this study, we recruited 10 patients with a confirmed AD diagnosis and 10 healthy controls (Table 5). MRI and mini-mental state examination (MMSE) tests were performed on all subjects at the Alzheimer’s Disease Center, Department of Neurology, Third Faculty of Medicine, Charles University, Prague, Czech Republic. For the purpose of the study, we used two groups of participants: (1) patients with mild cognitive impairment and dementia caused by AD according to NIA-AA criteria (McKhann et al., 2011; Albert et al., 2011) and (2) cognitively normal older adults. At the beginning of the study, there was a separate third MCI patient group, which was classified as the AD group later since

all the MCI group participants got diagnosed with AD by the end of the study. The AD diagnosis was made by an experienced neurologist through a thorough neurological and neuropsychological examination, functional assessments, blood work-up, brain MRI, single photon emission computed tomography (SPECT), and measurements of the total and phosphorylated tau proteins as well as -amyloid peptides in the cerebrospinal fluid upon the patients' consent to a lumbar puncture (Grothe et al., 2017). Most patients with the diagnosis were followed up for several years before they showed a cognitive and functional decline. Adults (controls) with normal cognitive abilities were recruited for the study at the University of the Third Age (adult education courses) of the Third Faculty of Medicine, Charles University, Czech Republic. These had normal MMSE scores (given recent Czech norms and limits) for mild AD (Bartoš et al., 2016). In the control group, only those who were over 70 years of age were selected in order to stay consistent with the age of the AD patients. For a more detailed description, see our previous article (Andica et al., 2020). The research was approved by the Ethics Committee of the Prague Psychiatric Center/National Institute of Mental Health and the Human Ethics Committee of the Third Faculty of Medicine, Charles University, Prague, Czech Republic, (Protocol No. 2016/3), and informed consent was obtained for all patients according to the Declaration of Helsinki.

Table 5. Characteristics of AD and control group.

	AD group	control group	p values
Numbers of participants	10	10	
Age at scan (years)	70.1 ± 6.5	67.6 ± 4.2	n.s
Education (years)	13 ± 1	14 ± 6	n.s
Male/female sex	6 / 10	5 / 10	n.s
MMSE score (0-30 pts.)	21 ± 3	29 ± 8	$p < 0.001$

Data are expressed as mean ± standard deviation. MMSE − the Mini-Mental State Examination, n.s. – not significant.

Instead of using automatic ROI learning for basal ganglia, we performed manual delineation of the structures. The advantage was the neuroanatomical delineation of structures of interest by experienced neuroanatomists instead of using existing maps.

The deterministic fiber tracking was conducted using DSI Studio, an open-source tractography software tool that analyzes brain connectivity. The tracking parameters selected for the fiber tracking were: the anisotropy threshold 0,05; the angular threshold 60 degrees; the step size 1 mm. Tracts of length less than 60 mm were discarded. A total of 1.000.000 seeds were placed. As a method for reconstruction was selected the q-space diffeomorphic reconstruction – QSDR, a model-free method. Whereas the model-based methods assume a particular diffusion distribution pattern or function, model-free methods estimate the empirical distribution of water diffusion without any assumption on the distribution. To these methods belong also diffusion spectrum imaging (DSI), q-ball imaging (QBI), and GQI. QSDR is the generalization of the generalized q-sampling imaging that allows to construct the spin distribution functions (SDF) in the standard MNI space, the Montreal Neurological Institute and Hospital coordinate system, and aims to preserve fiber orientations so that these can be used to conduct fiber tracking. The advantage of the model-free methods is that they do not presume a particular diffusion structure, and there is no risk of violation of the model. The calculation does not require complicated optimization or fitting and is therefore less affected by outliers. The downside are higher requirements on the number of diffusion samplings (Diffusion MRI Reconstruction, 2021). The spin distribution function (SDF) used in QSDR presents the amount of the spins undergoing diffusion in different orientations. In addition, this method aims to satisfy the conservation of diffusion spins, and the transformed SDFs can be used to conduct fiber tracking (Yeh et al., 2011). In QSDR, DSI Studio first calculates the QA mapping in the native space and then normalizes it to the MNI QA map (Diffusion MRI Reconstruction, 2021). QA is less sensitive to the partial volume effects of crossing fibers and free water compared to GFA calculated from an ODF function. For the tractography we decided to use the q-space diffeomorphic reconstruction, since Yeh and Tseng suggested that the transformed spin distribution function used in the QSDR could resolve fiber orientations in the crossing regions. In this way, we hoped to achieve more accurate results than with reconstruction methods using the orientation distribution function (Yeh et al., 2011). Through the fiber tracking and diffusion parameters, such as GFA, we obtained information about the WM and its damage. GFA, a value that highly correlates with FA, is a widely accepted quantitative measure of microstructural integrity (Liu et al., 2010). Reduced fractional anisotropy, and therefore GFA, is generally regarded as a sign of disrupted fiber tracts and demyelination, sensitive in the early detection of changes in white matter microstructure (Pasi et al., 2016). However, the limitation of GFA represents

its vulnerability to the partial volume effects of crossing fibers and therefore, its value decreases in fiber crossing or voxels with CSF partial volume (DSI-Studio; Fritzsche et al., 2010).

3.8 Statistics

3.8.1 CS and PCS length measurement in patients with schizophrenia and controls

For the purpose of general morphology, we fused all the subparts of each measurement into one number and did the overall statistics. For the more detailed view of morphology, we performed separate statistics for each part of the parcellation of the sulci.

Overall length differences between patients with schizophrenia and controls in the non parcellated PCS and CS were calculated by t-test for groups, and separately for cingulate sulcus right (CS R) and left (CS L) and paracingulate sulcus right (PCS R) and left (PCS L). The differences in the length of the CS (1, 2, and 3) as well as PCS (0, 1, and 2) between patients with schizophrenia and controls were calculated by nonparametric Mann–Whitney U test and Kruskal–Wallis test (because of unequal numbers of subjects in each category). ROC Curve Analysis was performed by an online ROC analysis web-based calculator with the data format 5 selection. ROC curve analysis was performed for the CS L and the PCS R only (because of the significant t-test). The differences between patients with schizophrenia and controls in their distribution within CS and PCS morphology were evaluated separately for the left and right hemispheres by a chi-squared test of the null hypothesis.

The Cochran–Mantel–Haenszel test (bilateral) was used to calculate the null hypothesis, similarly to the chi-squared test, but with the sum of the left and right hemispheres results. The differences between groups were also assessed in a formalized statistical model of GAM (generalized additive model) of semiparametric nature, which allowed for careful adjustment of the group (control versus schizophrenia) effect to sex and age (age effect was modeled by penalized spline with penalty coefficient estimation via generalized cross validation). GAM and ANOVA/ANCOVA modeling, chi-squared and Cochran–Mantel–Haenszel testing was done in the R environment (R Core Team, Vienna, Austria).

Other statistics were calculated in Statistica v.6 software (StatSoft, Tulsa, OK, USA) and the ROC curve analysis by an online program (http://www.rad.jhmi.edu/jeng/javarad/roc/JROCFITi. html). Statistical significance was commented at the 5% level ($p < 0.05$). Adjustment for Sex and Age Adjustment for age and sex was performed by the generalized additive model for both patients with schizophrenia and controls for the left and the right side in the CS (1, 2, and 3) and the PCS (0, 1, and 2).

3.8.2 Optimal hippocampal slice for hippocampal shrinkage identification on MRI

A T-test for independent groups was used to calculate differences between the control and AD groups (grouping factor) and left and right sides (variables). The T -test was calculated separately for absolute hippocampal areas and volumes, hippocampal areas normalized to brain areas at CA and hippocampal volumes normalized to TIV. The T-test was used also for calculation of differences in demographic characteristics between the control and AD groups (mean ± standard deviation). Cohen's d test, AUC-ROC, and comparison of ROC curves evaluated differences between absolute and normalized measurements, separately for the left and right sides. The T-test was calculated in Statistica v10 software, Cohen's d test in online Effect Size Calculator (https://lbecker.uccs.edu/), and AUC-ROC test in MedCalc v. 19.2.1. Statistical significance was accepted at $p \leq 0,05$.

3.8.3 Basal ganglia and surrounding white matter compensatory changes in AD

The statistical analysis was performed using the STATISTICA 13 software and the R statistical computing environment. The two-way ANOVA with repeated measures was applied for the analysis of the two independent groups (the AD patients and controls) and the two dependent variables (the left and the right side). The Wilks lambda test was used to evaluate the differences between the AD and control groups with the left and right sides as variables for both the DTI analysis and the FreeSurfer volumetric analysis. Pearson correlation coefficients were calculated to assess the relationship between the measures taken for the same person at different locations. Subsequently, we tested the differences in these correlations computed in the AD and control groups separately, using the Fisher z-transform and the two-sided test. In particular, we tested the AD versus control difference in correlations for both the number of tracts and the connectivity characteristics,

comparing—(i) the laterality (correlating the left and the right value of the same patient) of the putamen, pallidum, and the caudate, (ii) the structure (correlating the putamen, pallidum, and the caudate, separately for the left and right hemisphere), and then (iii) the structure segmentation volume (correlating the brain segmentation volumes in the putamen, pallidum, and the caudate, separately for the left and right hemisphere), plus (iv) the number of tracts/connectivity related to the volume of the putamen, pallidum, and the caudate. We acknowledge that different characteristics (like the number of tracts on the left and on the left) might be, to some extent, correlated.

4. Results

4.1 CS and PCS structural difference in patients with schizophrenia and controls (study no.1)

Characteristics of schizophrenia patients, controls and demographic data are stated in section 2.1

4.1.1 Length of CS and PCS without parcellation

Overall length differences of the CS and the PCS are shown in Table 6. The right hemisphere PCS was significantly longer in patients with schizophrenia compared to controls (19.4 ± 10.2 mm vs 12.1 ± 12.4 mm).

Table 6. Left and right CS and PCS without parcellation overall length differences between schizophrenia patients and control groups. The data are presented as mean values ± SD in mm. Statistical significance was calculated by t-test for groups.

Brain structures	Patients length (mm)	Controls length (mm)	p values

Left cingulate sulcus	112.4 ± 16.3	111.5 ± 18.8	n.s.
Right cingulate sulcus	114.7 ± 22.7	116.6 ± 24.4	n.s.
Left paracingulate sulcus	16.1 ± 9.1	14.4 ± 8.7	n.s.
Right paracingulate sulcus	19.4 ± 10.2	12.1 ± 12.4	$p<0.001$

4.1.2 Length of parcellated CS (1, 2 and 3) and PCS (0, 1 and 2)

Detailed analysis of the morphological subtypes of the CS and the PCS and their lengths in schizophrenia patients and controls are shown in Table 3 (chapter 2.3). The length of CS3a in the left hemisphere was significantly longer in patients with schizophrenia (53.8 ± 25.7 vs 32.7 ± 19.4 mm in controls) but in CS3c it was reversed - longer in controls (52.5 ± 22.5 mm) compared to schizophrenia patients (36.2 ± 12.9 mm) but without significance. The length of PCS0 in the right hemisphere was significantly longer in patients with schizophrenia (11.7 ± 5.2 mm) compared to controls (6.2 ± 6 mm), (it was not present at all).

4.1.3 Incidence and distribution of patients and controls between CS and PCS morphology types

Table 7 shows the differences in numbers of patients with schizophrenia and controls for each CS and PCS morphology type and incidence of distribution of particular sulcal patterns within CS and PCS morphology. Higher incidence of appearance in patients compared to controls in CS1, PCS0 and PCS1 were observed in both hemispheres; lower incidence in patients was observed in CS3 in both hemispheres; in CS2 on the left there was more incidence in controls compared to patients, and the opposite held true on the right - more in patients compared to controls (PCS2 in both hemispheres was not present). The number of patients with schizophrenia who had concurrently present CS1 as well as

PCS1 in both hemispheres was 9 (8.7%). The number of patients with PCS1 L and concurrently present CS1 L was 25 (83%); PCS1 R and concurrently CS1 R was 28 (68%).

Table 7. Comparison of patients and controls with CS1, 2 and 3 and PCS0, 1 and 2 types of morphology based on Table 3. The numbers show incidences (absolute values) of a particular morphology type in between patients with schizophrenia and controls. N/A – not applicable due to zero or low numbers of presence.

	CS1 left/right	CS2 left/right	CS3 left/right	PCS0 left/right	PCS1 left/right	PCS2 left/right
Patients	61/58	2/30	6/5	63/51	30/41	N/A
Controls	6/5	17/19	19/19	34/32	8/8	N/A

4.1.4 Adjustment for age and sex performed by Generalized Additive Model

After the adjustment for age and sex, we found PCS on the right side to be significantly ($p<0.001$) larger for schizophrenic patients than for controls (by about 7.346 on average), PCS on the left was not significantly different between patients and controls ($p=0.304$). Similarly, CS did not differ significantly between patients and controls neither on right ($p=0.375$), nor on left side ($p=0.877$). Difference between PCS on the right and left (laterality of the PCS) was significantly larger for patients than for controls ($p=0.019$) – by about 5.587 on average. Analogous laterality for CS was not significantly different between patients and healthy controls for CS ($p=0.331$).

4.1.5 ROC analysis evaluation

ROC analysis was performed for statistically significant results of the length of the CS L and PCS R between patients and controls. For the CS L were estimates of binomial ROC parameters A = 0.097 with standard error (SE) (A) = 0.24, B = 1.36 with SE (B) = 0.19 and correlation (A, B) = 0.032. The area under the fitted curve was 0.52 with SE =

0.056, trapezoidal (Wilcoxon) area = 0.51 with estimated SE = 0.054. For the PCS, R were estimates of binomial ROC parameters A = 0.63 with SE (A) = 0.31, B = 1.58 with SE (B) = 0.26 and correlation (A, B) = 0.14. The area under the fitted curve was 0.63 with SE = 0.06, trapezoidal (Wilcoxon) area = 0.63 with estimated SE = 0.055 (Figure 5). Therefore, ROC analysis suggests that the practical classification of schizophrenia patients and controls based only on the length of the CS L and PCS R is (obviously) far from being perfect.

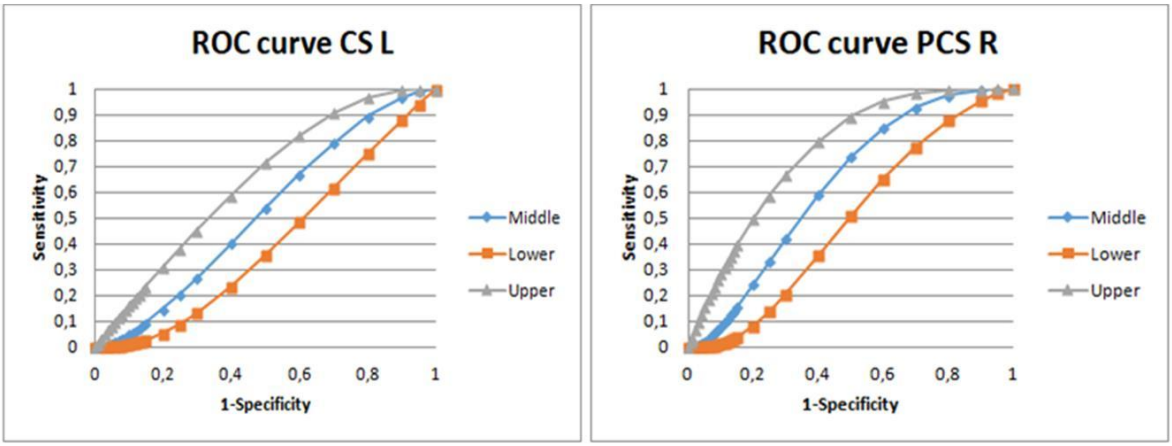

Figure 5. ROC curve analysis for length differences in left cingulate sulcus (CS L) and right paracingulate sulcus (PCS R) in schizophrenia patients vs controls without morphological parcellation. The area under the fitted curve was 0.52 with SE = 0.056 (CS) and 0.63 with SE = 0.06 (PCS).

4.2 Hippocampal optimal slice on frontal section for the visual assessment of the atrophy in AD patients (study no. 2)

Characteristics of participants and group comparisons are stated in section 2.4.

4.2.1 Absolute Hippocampal Area and Volume

Hippocampal areas in the optimal slice on the left and right in the control group were significantly higher than those in the AD group ($p < 0.001$). Hippocampal volumes on the left and right in the control group were significantly higher than those in the AD group ($p < 0.001$), (Table 8).

Table 8. Absolute and normalized hippocampal areas and volumes in Alzheimer disease patients and controls.

Absolute hippocampal areas in the optimal slice on the left and right are in mm^2. Absolute hippocampal volumes on the left and right are in mm3. Normalized hippocampal areas of the optimal slice to the brain area at anterior commissure on the left and right and normalized hippocampal volumes to total intracranial volume (TIV) on the left and right are in percentages. All values are expressed as means ± standard deviations, SE means standard error of AUC (ROC).

Hippocampal measures	AD patients	Controls	p values	Cohen´s d	AUC (SE)
Absolute measures (mm^2, mm^3)					
Area of the optimal slice on the left	118.1 ± 38.8	181.1 ± 25.7	< 0.01	1.91	0.91 (0.0331)
Area of the optimal slice on the right	112.1 ± 40.2	169.6 ± 29	< 0.01	1.64	0.87 (0.039)
Volume on the left (FreeSurfer)	2651 ± 746	3677 ± 948	< 0.01	1.2	0.86 (0.0486)
Volume on the right (FreeSurfer)	2777 ± 930	3761 ± 760	< 0.01	1.16	0.83 (0.0506)
Normalized measures (%)					
Area of the optimal slice on the left to brain area at anterior commissure	45.5 ± 11.8	63.6 ± 8.7	0.01	1.75	0.89 (0.034)
Area of the optimal slice on the right to brain area at anterior commissure	43.2 ± 13.3	59.5 ± 8.5	< 0.01	1.46	0.85 (0.0416)
Volume on the left to TIV (FreeSurfer)	0.29 ± 0.09	0.35 ± 0.08	0.01	0.7	0.73 (0.061)
Volume on the right to TIV (FreeSurfer)	0.31 ± 0.12	0.42 ± 0.14	< 0.01	0.84	0.78 (0.0551)

4.2.2 Normalized Hippocampal Area and Volume

Normalized hippocampal areas on the left and right in the control group were significantly higher compared to the AD group ($p < 0.001$). Normalized hippocampal volumes on the left and right in the control group were significantly higher compared to the AD group ($p < 0.001$), (Table 8).

4.2.3 Comparison of Absolute and Normalized Hippocampal Areas and Volumes

Normalized hippocampal areas as well as normalized hippocampal volumes did not differ significantly from corresponding absolute hippocampal areas and volumes ($p > 0.5$), (Table 9).

Table 9. No differences were found between absolute and normalized measures using comparisons of areas under the receiver operating characteristic curves

Absolute vs normalized hippocampal measures	p value
Area on the left	0.7
Area on the right	1.0
Volume on the left	0.9
Volume on the right	0.5

4.3 Compensatory changes of the BG gray and/or surrounding white matter in patients with AD compared to controls (study no. 3)

The age, education, sex, and MMSE score comparison between the AD patients and the healthy controls are stated in section 2.7.

4.3.1 DTI Analysis

Differences between the AD patients and the healthy controls were observed only in the NT and the normalized quantitative anisotropy (nQA). There were no significant differences in the TL, TV, and QA, as reported in Table 10.

Table 10. Overview of DTI parameters in patients with Alzheimer's disease and controls. NT = number of tracks, TL = tract length, TV = tract volume, QA = quantitative anisotropy, nQA = normalized quantitative anisotropy, GFA = generalized fractional anisotropy, unit = stands for absolute numbers, AD = Alzheimer's disease patients, ctrl = healthy control group. Data are reported as mean values ± standard deviation (SD); * $p \leq 0.01$, ** $p \leq 0.001$.

	NT (unit)	nQA (unit)	TV (mm^3)	GFA (unit)	QA (unit)	TL (mm)
Caudatum right ctrl	10945 ± 2816*	0.13±0.05	46594±16341	0.1±0.004	0.6±0.13	71 ± 11.1
Caudatum right AD	7667 ± 3557*	0.17±0.05	39382±18303	0.09±.006	0.62±.13	68.6 ± 15
Caudatum left ctrl	13873±3813	0.13±0.05	55388±16471	0.1±0.005	0.61±.13	77.6±8.1
Caudatum left AD	10527±5558	0.18±0.06	46135±21453	0.1 ±0.01	0.66±.15	74.6±16.2
Pallidum right ctrl	18202±3649**	0.15±0.06*	87140±30651	0.11±0003	0.68±0.1	110±16.8
Pallidum right AD	24882±5633**	0.21±0.05*	107239±23390	0.11±0.003	0.74±0.14	115.8±16
Pallidum left ctrl	20728±4002	0.15±0.06*	92296±23687	0.11±0.005	0.7±0.09	116.3±13.4
Pallidum left AD	24105±6108	0.21±0.05*	102759±23521	0.11±0.005	0.74±0.15	117.8±19.3
Putamen right ctrl	27172±5618**	0.13± 0.05*	102896±35726	0.1±0.004	0.62± 0.12	98.2± 15.9
Putamen right AD	38715±9724**	0.19± 0.05*	127691±30643	0.1±0.005	0.7±0.12	104 ± 9.7
Putamen left ctrl	35368±4250*	0.15± 0.06*	115491±23729	0.1±0.004	0.68± 0.11	104.6± 11.3
Putamen left AD	42603±9387*	0.2±0.05*	128184±29395	0.1±0.007	0.74± 0.16	107.8± 15

4.3.2 Number of Tracts (NT)

Compared to the controls, the patients with AD (AD SD/ctrl SD) showed decreased NT in the right caudate (7667 ± 3557/10,945 ± 2816) and increased in the right pallidum (24,882 ± 5633/18,202 ± 3649), the right putamen (38,715 ± 9724/27,172 ± 5618), and the left putamen (42,603 ± 9387/35,368 ± 4250), (Figure 6, Table 10).

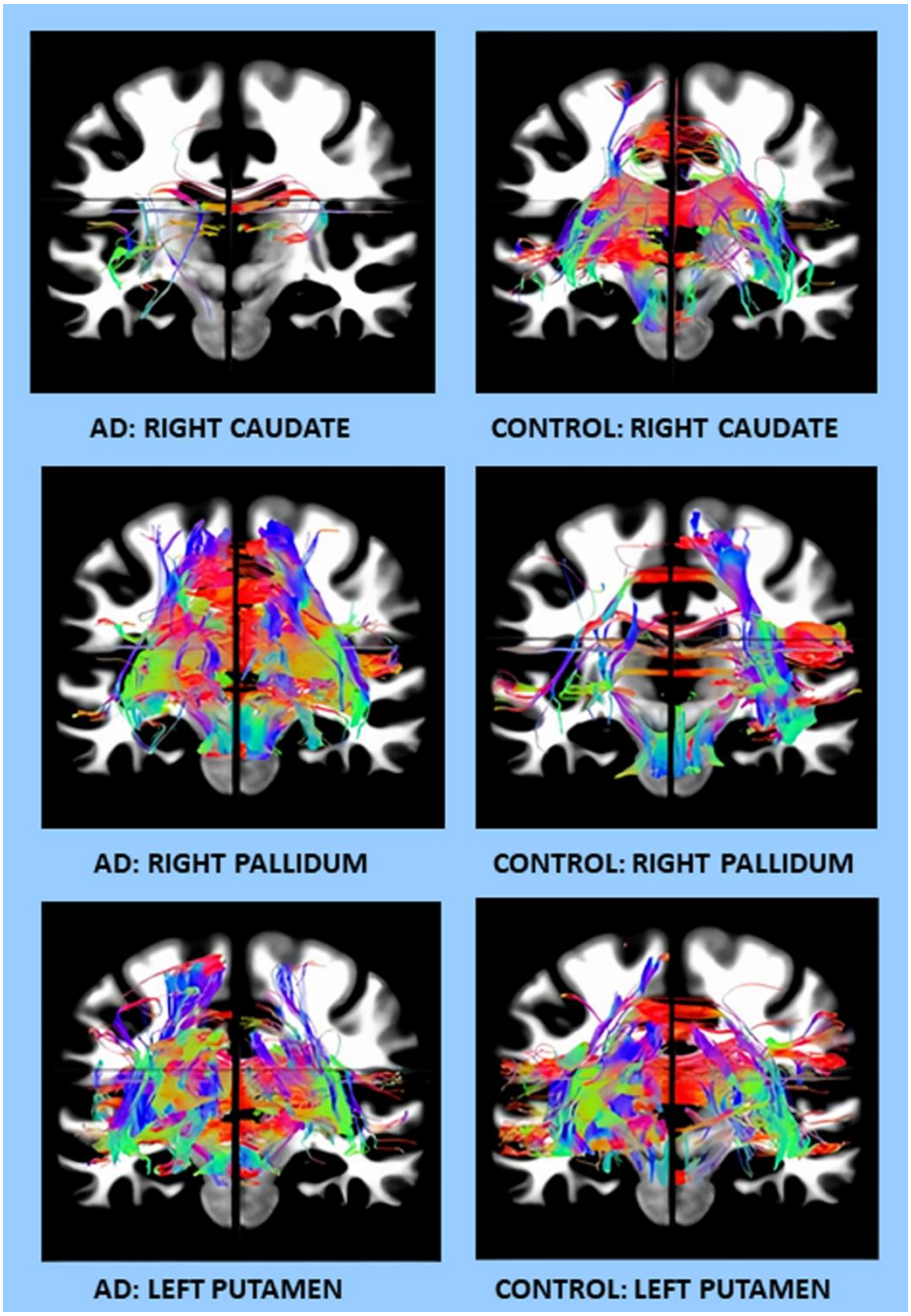

Figure 6. Examples of DTI changes in the AD patients compared to controls on coronal sections for different brain region (right caudate, right pallidum and left putamen).

4.3.3 Normalized Quantitative Anisotropy (nQA)

Patients, compared to controls, showed higher nQA values in the right pallidum (0.21 ± 0.05/0.15 ± 0.06), left pallidum (0.21 ± 0.05/0.15 ± 0.06), right putamen (0.19 ± 0.05/0.13 ± 0.05), and the left putamen (0.2 ± 0.05/0.15 ± 0.06), (Table 10).

4.3.4 FreeSurfer Volume Analysis

The differences between the patients with AD and the controls were observed in the volume of the left and right putamen and in the nucleus accumbens area. On the other hand, no significant differences were observed in the left and right caudate nucleus and also in the brain segmentation volume. Further, a volume decrease in the right and left putamen was found in the AD patients in comparison to controls (respectively, 3487.3 m^3 vs. 4283.9 m^3 and 3656.5 m^3 vs. 4302.2 m^3), as reported in Table 11.

Table 11. Difference in volumes of basal ganglia structures and total brain volume in Alzheimer's disease patients and controls estimated by FreeSurfer. Values are reported in μm^3, n.s.= not significant.

Structure	AD patients	controls	p-value
left caudate	3016.7	3304.8	n.s.
left putamen	3656.5	4302.2	p = 0.01
left pallidum	1843.1	1747.9	n.s.
right caudate	3043.4	3321.4	n.s.
right putamen	3487.3	4283.9	p = 0.01
right pallidum	1897.5	1813.8	n.s.
brain segmentation volume	10.1x105	10.37x105	n.s.

4.3.5 Pearson Correlation Coefficients

Significant changes in the correlations of several characteristics were observed between the patients with AD and the controls. In particular, the correlation between the number of tracts in the left pallidum and the number of tracts in the left caudate was 0.609 for the controls and -0.493 for the AD patients. The difference was highly significant, with the *p*-value = 0.019. The correlation between the number of tracts in the right pallidum and the number of tracts in the right caudate was 0.691 for the controls and -0.566 for the AD patients; hence, their difference was highly significant, *p*-value = 0.005. The correlation between the right putamen connectivity and the right putamen volume was -0.367 for the controls and 0.678 for the AD patients; hence, their difference was significant, with the *p*-

value = 0.04. The qualitative differences in correlation patterns between the AD patients and the controls are shown graphically in Figure 7.

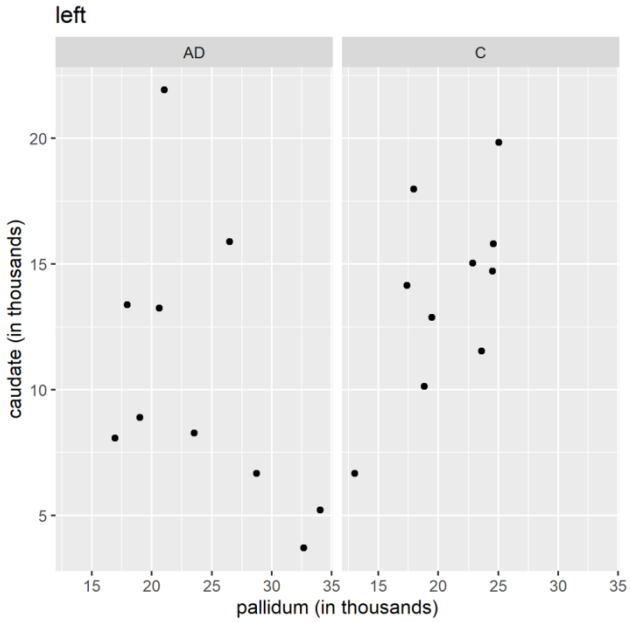
left
AD
C
caudate (in thousands)
pallidum (in thousands)

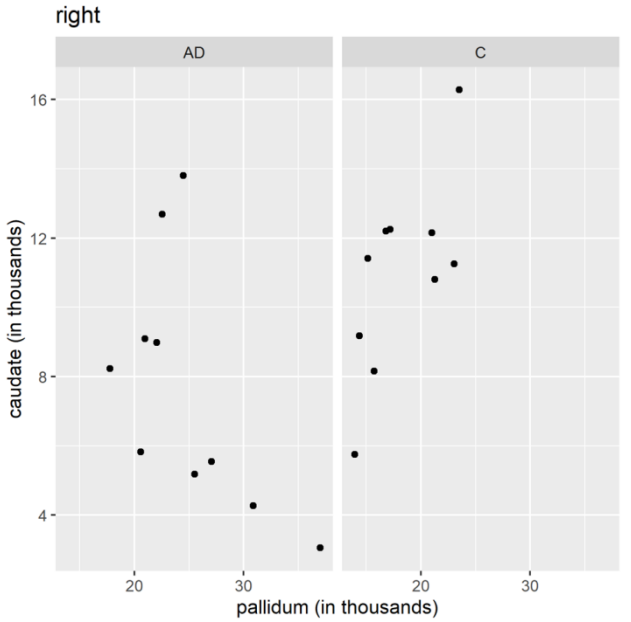
right
AD
C
caudate (in thousands)
pallidum (in thousands)

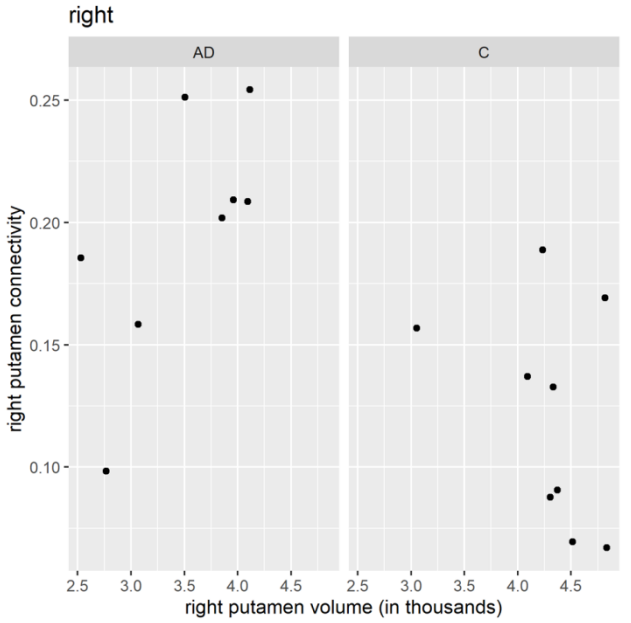
right
AD
C
right putamen connectivity
right putamen volume (in thousands)

Figure 7. Comparison of number of tracts, connectivity and volume in caudate, pallidum and putamen (Pearson correlation coefficients). Upper panels: left pallidum vs left caudate, number of tracts. Middle panels: right pallidum vs right caudate, number of tracts. Bottom panels: right putamen volume vs right putamen connectivity. AD - Alzheimer's disease patients; C - controls. Values on x and y axis are reported in absolute units.

4.4 Asymmetric nature of CNS changes in patients with schizophrenia, Alzheimer's disease and controls (studies no. 1-3)

Distribution of the CS and PCS morphotypes in patients with schizophrenia was different from controls. Parcellated sulcal pattern CS3a in the left hemisphere was longer in patients (53.8 ± 25.7 mm vs. 32.7 ± 19.4 mm in controls, $p < 0.05$), while in CS3c it was reversed—longer in controls (52.5 ± 22.5 mm as opposed to 36.2 ± 12.9 mm, n.s. in patients). Non parcellated PCS in the right hemisphere were longer in patients compared to controls (19.4 ± 10.2 mm vs. 12.1 ± 12.4 mm, $p < 0.001$).

Hippocampal areas on the single optimal slice and hippocampal volumes on the left and right in the control group were significantly higher than those in the AD group. Normalized hippocampal areas and volumes on the left and right in the control group were significantly higher compared to the AD group.

A significant decrease in the number of tracts and general fractional anisotropy was found in patients with AD compared to controls in the right caudate nucleus, while an increase was found in the left and the right putamen. Further, a significant decrease in the structural volume of the left and the right putamen was observed. An increase in the white matter diffusion tensor imaging parameters in patients with AD disease was observed only in the putamen bilaterally. The right caudate showed a decrease in both the diffusion tensor imaging parameters and the volume in AD patients. The right pallidum showed an increase in the diffusion tensor imaging parameters but a decrease in volume in AD patients.

5. Discussion

5.1 CS and PCS structural difference in patients with schizophrenia and controls (study no.1)

Numerous studies in literature document the relationship between the morphological changes of the central nervous system and schizophrenia, e.g. cortical areas (Heckers, 2001), amygdala (Breier et al., 1992), hippocampus (Artiges et al., 2006) and others (Garrison et al., 2019), but they are not suitable for morphological diagnosis of schizophrenia because of their non-specificity and frequent anatomical variability.

The CS and the PCS are two regions found within the ACC on the medial side of the brain hemisphere. Morphological variability of the PCS was described for example in (Garrison et al., 2015). Specificity of the morphological changes in ACC vs other cortical areas were described by (Fornito et al., 2008; 2009). Variability in the CS organization in human adult and fetal cadavers was described by (Marinescu et al., 2018). The CS structure was analyzed in 6 groups of adult brains whose medial hemisphere was parcellated into I-III sectors, clockwise to the CS course. The major differences in the CS organization could be summarized into the following observations: in sector I the subgenual part of callosal body varies in the numbers and shape of the CS infoldings, in sector II there is broken trajectory of the CS by the dorsal cingulate-frontal infolding, and in sector III the trajectory is sinusoid and there is a convoluted aspect of the marginal branch. It is still difficult to account for these variations on the MRI where tiny details of the CS neuroanatomy are often blurred by the arachnoid.

5.1.1 Distribution of CS and PCS morphological patterns

We found significant differences between schizophrenia patients and controls in all types of the CS (1, 2 and 3) and the PCS (0, 1, and 2). Left-right asymmetries were not significant with the exception of PCS0 and PCS1 in schizophrenia patients. The most common in schizophrenia patients and controls was the presence of PCS0 morphology, followed by PCS1 and PCS2. Schizophrenia patients were found to have the most common

CS1 morphology, followed by CS2 and CS3. This was in contrast with the control group where the most common morphology was CS3 and CS2, followed by CS1. At least for the distribution of the morphological patterns of both PCS and CS, there are significant differences between schizophrenia patients and controls. The trend of these morphological distributions in healthy subjects described by (Wei et al., 2017) was similar to our results (although the effects of sex and handedness were included as well).

5.1.2 Length of the PCS

We found significantly longer non-parcellated PCS in the right hemisphere of schizophrenia patients compared to the control group. This is based on statistically significant differences only in the right PCS0 part in schizophrenia (see Table 3). Schizophrenia patients were reported to have a frequent absence of the left PCS. In healthy volunteers, prominent or present PCS was described more frequently in the left hemisphere compared to the right. On the contrary, schizophrenia patients were found to have no significant asymmetry and types prominent or absent. These all were found with the same frequency (Yücel et al., 2001; Le Provost et al., 2003). In our study, we found more often similar PCS1 in controls in the left hemisphere compared to the right. However, we did not observe enough cases of PCS2 (prominent) to create valid statements about their frequency neither in control nor in schizophrenia patients. We observed left-right asymmetry in the PCS length in schizophrenia patients only and not in the control group. Leftward asymmetry was observed only in PCS0 (absent) and rightward asymmetry in PCS1 (present). This is also in contrast to the study by (Le Provost et al., 2003; Artiges et al., 2006) measured the morphology of the PCS in relation to fMRI hypoactivation in the ACC in 13 patients with schizophrenia and 16 healthy controls. They did not observe a difference between healthy subjects and patients with the PCS (PCS1 and PCS2 in our classification), but patients with schizophrenia exhibited significant hypoactivation of the ACC, where the PCS was absent (PCS0 in our classification). According to our data, PCS0 was present in both schizophrenia patients and controls with the highest statistical occurrence, so that we support the notion that hypoactivation may take place even in the size of our studied group (patients with schizophrenia n=93 and control group n=42). The

advantage of the Image J program is manual delineation, by which it is possible to distinguish the length of the PCS0 from 0 to 2cm.

Shorter PCS (without parcellation) was observed in patients diagnosed with psychotic disease having hallucinations; they had shorter PCS compared to non-hallucinating psychotics and healthy controls (Garrison et al., 2019).

In summary, we show that there is a reverse tendency in the PCS0 and PCS1 length between schizophrenia patients and controls. In PCS0 type morphology ("absent" type according to Yücel´s nomenclature) we found a lower number of schizophrenic patients with the absent PCS compared to controls, regardless of the hemisphere (left 67% patients and 81% controls; right 55% patients and 76% controls). This finding is consistent with reports of (Yücel et al., 2001; Le Provost et al., 2003). We found the opposite for PCS1 - a higher number of patients with schizophrenia having PCS1 type of morphology ("present" type according to Yücel´s nomenclature), (left 32% patients and 19% controls; right 44% patients and 19% controls) compared to controls. These differences may explain the inconsistency between the observed leftward PCS hemispheric asymmetries in schizophrenia and healthy controls (Fornito et al., 2008; Noga et al., 1995) versus reduced PCS asymmetries in schizophrenia patients (Yücel et al., 2002; Le Provost et al., 2003) because of the intrinsic differences in both the CS and the PCS.

5.1.3 Length of the CS

It appears in schizophrenic patients that the CS is generally uninterrupted when viewed from the sagittal section, while in the control group this was rarely seen. On the contrary, the control group was almost equally split into half of participants having one and two interruptions of the CS. In other words, in the CS there is a reversed trend in the number of participants as for increase/decrease of the number of interruptions (in control groups the number of interruptions rises, while in schizophrenia patients it declines). It appears that it is an advantage to have an interrupted CS as opposed to the uninterrupted CS.

In summary, we show that there is a difference in length between CS1 and CS2 in schizophrenia patients and controls. In CS1 type morphology ("uninterrupted" type), we found a higher number of patients with schizophrenia with uninterrupted CS compared to controls, regardless of the hemisphere (left - 66% patients and 14% controls; right - 62% patients and 12% controls). On the contrary, in CS2 (one interruption) there was a higher number of controls compared to patients (left - 41% controls and 26% patients; right - 43% controls and 32% patients). In CS3, similarly to CS2, there was a higher number of controls than patients (left - 45% controls and 6% patients; right - 45% controls and 5% patients).

The length of the left CS3a was significantly longer in patients with schizophrenia, while the length of CS3c was longer in controls; CS3b did not differ between the groups. From the perspective of the study by (Marinescu et al., 2018), CS3a corresponds to sector I and CS3c to sector III. CS3a is close to the rostral area of the callosal body with the variability of connective infolding between the gyrus cinguli and the parolfactory area and the infolding between gyrus cinguli and the rostral gyrus that continues with the gyrus frontalis superior. CS3c is the continuation of the main sulcal line into the marginal part of CS that also shows variability in the posterior cingulate-parietal connective infolding (Marinescu et al., 2018).

The length of the CS and PCS in the healthy population was described, for example, by (Fornito et al., 2008), however, there is no such data in schizophrenia patients. We did not observe any gross morphological abnormalities of the CS and the PCS in schizophrenia patients, so we presume that the overall shape and morphology are not valid as clinical markers for the differential diagnosis of schizophrenia. On the contrary, the CS and the PCS length differ between both groups significantly, specifically, a decrease in length of the CS in schizophrenia patients is compensated by the length increase in the PCS. We found this valid for the right hemisphere only. Interestingly, we discovered two opposite trends in the left hemisphere. The length of CS3a was significantly longer in schizophrenia patients, while CS3c was significantly longer in control. Our results partially correspond to the hypothesis of (Rametti et al.,2010), who studied the maximal depth and volume of the anterior cingulate sulcus and the PCS in 23 patients and 24 controls. However, they do not define the borders of the main measured area (the ACC) precisely in their study. The other difference is, they used automated voxel based morphometry measurements with manual correction while we did all the measurements manually. The

study found significant decrease in volume in the anterior cingulate sulcus in the left hemisphere and significant increase in the PCS volume in the right hemisphere of the patients with schizophrenia compared to controls (Rametti et al., 2010).

The limitation of our study is the analysis of the sulcal shape that was performed in the sagittal plane view only. This way we may have missed invaginations of the CS in the white matter in lateral direction. This could have led to labeling of some sulci (CS2 and CS3) as interrupted, although they could have been present, if viewed on the coronal sections. Also, general atrophy of the white matter in schizophrenia patients could lead to merging of sulcus as a result of smoothening and unification of the surface cortical areas (Kubicki et al., 2005). This observation could be supported by controls, who have relatively longer, although interrupted courses of the CS. Another limitation is the demographic differences between control group and schizophrenia group, thus analyzing a larger population sample may improve the understanding of CS and PCS morphology.

Delineation of the CS and PCS was done on MRI scans in sagittal projection - this is what clinicians would use, too. The problem with delineation of the ACC is that it is based on the cytoarchitectonic, post-mortem diagnosis. The posterior part of the ACC in the transition to the posterior cingulate gyrus (PCC) is difficult to evaluate on the MRI (Rushworth et al., 2004). For this reason it is not usable as a clinical diagnostic tool. We could not account for precise anatomical details of both sulci delineation, as described by e.g. (Marinescu et al.,2018), because their study was done on post mortem brain tissue with much more anatomical details. Nevertheless, we described the Methods section in great detail so that it can be used as guidance for both sulci delineation on the MRI scans, which would minimize bias in interpretation of their occasionally variable course.

We analyzed each response separately, without corrections to multiple comparisons. This corresponds to univariate/marginal analyses and might lead to some inflation of falsely positive results. As we intend the study as exploratory, or pilot study in the uncovered area, we do not want to be overly conservative. On the other hand, it is certainly in place to verify the significant findings on independent samples in future.

Up to date there is no agreement in literature as to whether education matching should be done in comparative schizophrenia studies. Matching subject groups according to age, gender and education level is common practice aimed at obtaining a representative sample in the context of comparative group studies. Indeed, it has been shown that

education level impacts brain morphology (Ge et al., 2019), and education level matching has been done in previous studies (Duan et al., 2015). However, a recent meta-analysis by Crossley et al., (2022) confirmed substantial education level differences between schizophrenia patients and the healthy population, thereby demonstrating that education level matching could lead to suboptimal representation of group samples. Therefore, similarly to Delvecchio et al., (2018), we matched the demographic data according to gender and age but not the years of education.

5.1.4 Practical use of CS and PCS length as a support tool for schizophrenia diagnosis

The data in Table 3 could be useful as a guide for further MRI studies of schizophrenia. Depending on the MRI morphological typology of the CS and the PCS subsets in patients it is possible to predict the following combinations of the medial hemisphere sulcal appearance: 1) absent PCS and one of the CS type (1, 2, 3); 2) present PCS and one of the CS type (1, 2, 3); 3) prominent PCS and one of the CS type (1, 2, 3). Out of these only concurrent unilateral presence of PCS1 and CS1 in the left or the right hemisphere suggests a higher probability of schizophrenia. All other combinations point at the lack of disease. The morphological differences that we documented may potentially be of use as support tools demonstrating the differences present in schizophrenia. However, further research is required prior to implementing morphological measures as a support tool for schizophrenia diagnosis.

Brain ultrasound and magnetic resonance images of fetuses 18-23 gestational weeks showing the structure of the sulcus cinguli suggest the possibility of comparing morphology between adult brains and possible changes in the ACC region from the prenatal period (Ghai et al., 2006). The deviation in cortical folding within cingulate area suggest neurodevelopmental alterations within this area albeit incomplete understanding of cellular, genetic, and experience-dependent plasticity behind aberrant cortical folding precludes for the time being conclusive statements about the neurobiological underpinnings of those changes. Given current status of knowledge, further elucidation of the role of genes involved in driving the maturational trajectories of cortical patterning and the impact of events that disrupt fetal neurodevelopment is prerequisite for whole

understanding of those processes inflicting upon composition of cortical architecture in schizophrenia.

5.2 Hippocampal optimal slice on frontal section for the visual assessment of the atrophy in AD patients (study no. 2)

Our results show that hippocampal shrinkage in the AD patients could be reliably evaluated from the single coronal slice of the brain on the MRI and without normalization to the TIV or other brain measures. We combined manual and automated (FS) delineation of the hippocampus. It was found that there is high reliability and agreement between FreeSurfer and manual hippocampal protocols (Fung et al., 2019). Our slice is at the level of the memory processing (ventral hippocampus), (Takashima et al., 2006) but not at the level of 3D spatial navigation (dorsal hippocampus), (Porter et al., 2018). Other studies used several slices and stages of Alzheimer's disease development but without having MRI slices precisely defined by space position of the anatomical structures (Li et al., 2019). These slices often seem to be localized at the level of the dorsal hippocampus. Numerous protocols in clinical studies with Alzheimer's disease patients often use the hippocampus to brain TIV normalization (Estévez-Santé et al., 2020; Hu et al., 2015). However, our results show that normalization is not necessary in order to evaluate hippocampal shrinkage as part of diagnosis. Possible mistake of total intracranial volume estimation by FS and suggestion for evaluation of intracranial volume by two intracranial areas and width are mentioned in (Klasson et al., 2018a; Klasson et al., 2018b). No effects of age-related changes on the MRI were observed in the temporal lobe width and temporal horn width measurements both on right and left sides (Salk et al., 2014). Temporal horn volumes and temporal horn index measurements in AD were significant in AD compared to controls but not in MCI (Giesel et al., 2006). On the other hand, temporal horn expansion was found more reliable to predict conversion from MCI to AD than hippocampal volume alone because of smaller changes in it compared to the size of the temporal horn (Macdonald et al., 2013). Other variants of a 2D single brain slice from which we could derive measurements of hippocampus atrophy represent a study that measured manually 3 regions on coronal MRI at the level of the interpeduncular fossa to calculate the Medial Temporal Atrophy index (Menendez-Gonzalez et al., 2014). Similarly, our design offers only one simple and easily distinguishable marker that is

enough for clinicians to analyze the optimal slice for Alzheimer's disease MRI diagnosis. We also measured the area of the coronal slice of the skull at the same level as the area of the brain (at CA) to do experimental area normalization to the brain/skull ratio. We found a significantly lower brain area/skull area ratio in the AD group compared to the control group. Furthermore, another experimental normalization of hippocampal areas (left and right) to the brain area/skull area ratio showed similar results as the hippocampus to area of brain in CA normalization — significantly lower in the AD group compared to the control one. The same results showed the brain volume/skull volume ratio and normalization of the hippocampal volumes to brain volume/skull volume ratio (unpublished results). We did not include the above-mentioned data in the article because of the similarity of results they revealed. The limitations of our study include the normalization style we used. We normalized left and right hippocampal areas and volumes to the total brain area at the level of CA and total intracranial volume. TIV normalization does not make a difference between left and right hemispheres so that it compares right and left hippocampal volumes to the volume of the whole brain. More precise and valuable for the statistics would be comparison of hippocampal areas and volumes (left and right) to the area and volume of the corresponding left and right hemispheres, but this is not widely accepted.

5.3 Compensatory changes in BG - hypertrophy of gray matter or surrounding white matter following progression of atrophy in other structures in patients with Alzheimer's disease (study no. 3)

DTI is challenging, and the fiber tract reconstruction depends on the quality of the diffusion data. The theoretical basics and a number of factors influencing the reconstruction results are covered in the literature (Jones and Cercignani, 2010; Borkowski et al., 2017). For example, the gradient field inhomogeneity causes artifacts that affect the results of the reconstructed fibers. The gradient field can be efficiently mapped using the b-matrix spatial distribution in DTI (BSD-DTI) technique to correct the magnitude and the direction of the diffusion gradient (Borkowski et al., 2018). In our study, the nQA parameter has been used for the fiber tracking (FT) instead of the FA due to the fact that QA-aided tractography has reached a better resolution and is less sensitive to partial

volume effects of the crossing fibers than the tractography based on the FA (Yeh et al., 2013). FA is defined for all the fiber populations within a voxel and suffers from the partial volume effect. Therefore, the data were reconstructed using the DSI studio with the GQI method. GQI is a free model that can be applied to any diffusion scheme that provides a quantitative anisotropy (QA) parameter, which is based on the spin distribution function (SDF) of diffusing water at different orientations. QA measures the spin density of anisotropy along a fiber pathway for each fiber population and contributes to more reliable tractography. QA can be normalized (nQA), which stabilizes the proton density across subjects (Zhang et al., 2013). An increase in values of the quantitative DTI parameters in theWMof the AD patients was observed only in the left and the right putamen, while their volumes were reduced compared to the controls. The right caudate showed, as expected, a decrease in both the DTI parameters and the volume in the AD patients compared to the controls. The right pallidum showed, similarly to the putamen, an increase in the DTI parameters but a decrease in volume in the AD patients compared to the controls. An increase in the values of the quantitative DTI parameters of theWMobserved in AD patients suggests the plasticity of specific tracts. The question is whether the whole process should be labeled as degeneration. Deposition of the amyloid plaques and deposits is typically present at the inferior part of the temporal lobe and the posterior cingulum (Grothe et al., 2017; Tucholka et al., 2018). These are also anatomical targets of the projections that undergo the WM hypertrophy or increase in the tract fibers on the DTI. Why is there a decrease in the number of tracts in the caudate nucleus but an increase in the pallidum and the putamen? When considering the loops of the BG circuits, the motor loop skips the caudate nucleus but not the pallidum and the putamen. On the contrary, the executive/associative loop of the BG skips the putamen but deploys the caudate nucleus (DeLong et al., 2007). Since the motor skills are not affected in the early and mid-stages of AD, while cognition and memory decline, the observed compensatory WM hypertrophy in the putamen and the pallidum does not seem to be effective even though it is present. Since the caudate nucleus inhibits the pallidum, the increase in the WM of the pallidum could be due to its spontaneous activation after the caudate atrophies. Given that the caudate is evolutionarily older compared to the relatively younger putamen (Grillner and Robertson, 2016) we hypothesize that the caudate could be the first to suffer the loss of structure and function. Thus, the putamen may not undergo neurodegeneration so easily; it could stay intact for longer and may, to some extent, substitute for the loss of function of the caudate. However, the observed caudate/putamen volume ratio in early caudate dysfunction in PD

patients suggests this is not the case (Pasquini et al., 2019). Although the WM compensatory changes in AD on the DTI were not described frequently, they were observed in PD (Sanjari et al., 2020), Tourette's syndrome (Jackson et al., 2011), schizophrenia, and bipolar disorder (Ji et al., 2019; Xekardaki et al., 2011). Interestingly, increased connectivity in the right caudate nucleus was observed in cognitively normal PD patients (Wright et al., 2020). Recently, we proposed that an increase in values of the quantitative DTI parameters of the WM in the subcallosal area and the paraterminal gyrus is an aftermath of the hippocampal atrophy (Kuchtová et al., 2018; Deeb et al., 2019). We now propose another structural/functional compensatory mechanism for hippocampal atrophy in AD in terms of the BG white matter volume increase. The reason for this compensatory hypertrophy could be their participation in the association loop of the BG circuit (association cortex — BG — thalamus — cortex). This circuit is responsible not only for motor skills but also for memory formation (emotional memory and positive reward reaction, episodic memory, and association cortices bound to memory formation). In AD, attention has been paid to the brain areas with clinically proven morphological atrophy (the hippocampus, various cortical areas, the brain stem, and others). Recently, there were attempts to include clinical diagnostics and atrophy of neuroanatomical heterogeneous areas, i.e. basal forebrain cholinergic system (Kilimann et al., 2014). We suggest another option: what if there are numerous compensatory shifts in motor/association/sensory and other brain structures, including the tracts in AD patients, detectable on the DTI (such as NT, TL, TV, QA, and GFA) that manifests by default when the atrophied primary memory circuits fail to work properly? Limitations of the study: A small sample size (10 subjects) of our study represents some limitations; the observed asymmetric changes may be the result of a small sample, and further study with more patients is needed to confirm our conclusions. White matter changes around the basal ganglia were not specifically parcellated into the afferents or the efferents, nor were they classified into any kind of intrinsic or extrinsic projections in regards to the cortex, the brain stem, or the diencephalon. This way, it was compared only to the sum of three-directional projections between the AD patients and the controls. For future research it would be good to compare the DTI-based tractography of separate tracts and pathways of the BG in AD patients and controls, the cortical ones in particular.

6. Conclusions

6.1 CS and PCS structural difference in patients with schizophrenia and controls (study no.1)

Our study expands previously documented morphological classification of the sulcal patterns within the anterior cingulate area, especially the quantification of various morphology types of cingulate and paracingulate sulcus in patients with schizophrenia and the healthy population. Based on our results on ACC parcellation (CS1, 2, and 3; PCS0, 1, and 2), it is possible to postulate that the concurrent presence of PCS1 and CS1 in the left hemisphere as well as, to some extent, in the right hemisphere suggests a higher probability of schizophrenia. However, concurrent presence of PCS1 and CS1 in the left and right hemisphere at once is not very frequent.

6.2 Hippocampal optimal slice on frontal section for the visual assessment of the atrophy in AD patients (study no. 2)

We present a simplified protocol for hippocampal atrophy evaluation on MRI in Alzheimer disease based on single optimal coronal slice analysis. In order to prove it, we measured the absolute area of the hippocampus at the single optimal slice and compared it with the normalized area of the same slice. We found no difference between the hippocampal absolute and normalized area in control and AD patients. Similarly, we did not find a difference between absolute and normalized hippocampal volumes. We found that estimation of hippocampal shrinkage in Alzheimer disease on MRI could be reliably done without normalization.

6.3 Compensatory changes in BG - hypertrophy of gray matter or surrounding white matter following progression of atrophy in other structures in patients with Alzheimer's disease (study no. 3)

Our data show there is an asymmetrical increase in the DTI parameters in patients with AD, which is consistent with our hypothesis stating that the same pattern may appear in other brain areas as well (which has not been proven yet). More specifically, a decrease in the volume of the left and the right putamen in the AD patients compared to controls was expected when measured by the FS. Interestingly, there was an increase in the NT in their proximity. If this was the effect of the compensatory changes (i.e. reduced volume of the structure and an increase in the amount of the WM fibers around it), then it remains unclear why the pallidum or caudate would not show a similar compensatory effect as well. Moreover, the timing of these changes remains unclear. Do they arrive prior to the decrease in the volume of the putamen and the increase in the white matter NT follows, or is it the other way around? Or rather, do all the changes occur relatively simultaneously?

7. Summary

Monitoring the parcellation and length of the sulcus cinguli and sulcus paracingularis in patients with schizophrenia shows a new possibility of using CNS morphometry in the auxiliary diagnosis of this disease. A limitation, however, is the variability of this area with respect to age and timing of diagnosis. Nevertheless, it relates well to the findings of gyrification patterning in the fetal period.

Determination of the optimal hippocampal section may be a useful tool for the neurologist's office, who, instead of tedious measurement of hippocampal area and volume, can use this methodology to easily assess hippocampal atrophy in patients with Alzheimer's disease.

Asymmetric changes in the gray matter of the basal ganglia and adjacent white matter suggest the possibility of compensatory hypertrophy in patients with Alzheimer's disease.

This finding supports a previous study in which compensatory hypertrophy of the area subcallosa and gyrus paraterminalis was observed in patients with Alzheimer's disease. Further measurements are needed in a larger sample of patients and controls to compensate for this theory.

7. Souhrn

Sledování parcelace a délky sulcus cinguli a sulcus paracingularis u pacientů se schizofrenií ukazuje novou možnost využití morfometrie CNS v pomocné diagnostice tohoto onemocnění. Omezením je však variabilita této oblasti s ohledem na věk a načasování diagnózy. Nicméně dobře to souvisí s nálezy morfologie gyrifikace ve fetálním období.

Stanovení optimálního řezu hipokampu může být užitečným nástrojem pro ordinaci neurologa, který místo zdlouhavého měření plochy a objemu hipokampu může pomocí této metodiky snadno posoudit atrofii hipokampu u pacientů s Alzheimerovou chorobou.

Asymetrické změny v šedé hmotě bazálních ganglií a přilehlé bílé hmotě naznačují možnost kompenzační hypertrofie u pacientů s Alzheimerovou chorobou. Toto zjištění podporuje předchozí studii, ve které byla u pacientů s Alzheimerovou chorobou pozorována kompenzační hypertrofie area subcallosa a gyrus paraterminalis. K průkazu této teorie jsou zapotřebí další měření na větším vzorku pacientů a kontrol.

8. Overview of the literature

1. ALBERT, M. S., DEKOSKY, S. T., DICKSON, D., DUBOIS, B., FELDMAN, H. H., FOX, N. C., GAMST, A., HOLTZMAN, D. M., JAGUST, W. J., PETERSEN, R. C., SNYDER, P. J., CARRILLO, M. C., THIES, B., PHELPS, C. H. The diagnosis of mild cognitive impairment due to Alzheimer's disease: Recommendations from the National Institute on Aging-Alzheimer's Association workgroups on diagnostic guidelines for Alzheimer's disease. *Alzheimer's & Dementia.* 2011, **7**(3), 270-279. ISSN 1552-5260. DOI: 10.1016/j.jalz.2011.03.008.

2. AMIEZ, C., SALLET, J., NOVEK, J., HADJ-BOUZIANE, F., GIACOMETTI, C., ANDERSSON, J., HOPKINS, W. D., PETRIDES, M. Chimpanzee histology and functional brain imaging show that the paracingulate sulcus is not human-specific. *Communications Biology*. 2021, **4**(1), 54. ISSN 2399-3642. DOI: 10.1038/s42003-020-01571-3.

3. ANDICA, C., KAMAGATA, K., HATANO, T., SAITO, Y., OGAKI, K., HATTORI, N., AOKI, S. MR biomarkers of degenerative brain disorders derived from diffusion imaging. *Journal of Magnetic Resonance Imaging*. 2020, **52**(6), 1620-1636. ISSN 1053-1807. DOI: 10.1002/jmri.27019.

4. ARTIGES, E., MARTELLI, C., NACCACHE, L., BARTRES-FAZ, D., LEPROVOST, J. B., VIARD, A., PAILLERE-MARTINOT, M. L., DEHAENE, S., MARTINOT, J. L. Paracingulate sulcus morphology and fMRI activation detection in schizophrenia patients. *Schizophrenia Research.* 2006, **82**(2-3), 143-151. ISSN 0920-9964. DOI: 10.1016/j.schres.2005.10.022.

5. BARTOŠ, A., GREGUŠ, D., IBRAHIM, I., TINTĚRA, J. Brain volumes and their ratios in Alzheimer´s disease on magnetic resonance imaging segmented using Freesurfer 6.0. *Psychiatry Research: Neuroimaging.* 2019, **287**(May), 70-74. ISSN 0925-4927. DOI: 10.1016/j.pscychresns.2019.01.014.

6. BARTOŠ, A., RAISOVÁ, M. The Mini-Mental State Examination: Czech Norms and Cutoffs for Mild Dementia and Mild Cognitive Impairment due to Alzheimer's Disease. *Dementia and Geriatric Cognitive Disorders*. 2016, **42**(1-2), 50-57. ISSN 1420-8008. DOI: 10.1159/000446426.

7. BERGER, A. Magnetic resonance imaging. *BMJ*. 2002, **324**(7328), 35. ISSN 0959-8138. DOI: 10.1136/bmj.324.7328.35.

8. BIGLER, E. D., BLATTER, D. D., ANDERSON, C. V., JOHNSON, S. C., GALE, S. D., HOPKINS, R. O., BURNETT, B. Hippocampal volume in normal aging and traumatic brain injury. *AJNR. American Journal of Neuroradiology.* 1997, **18**(1), 11-23. ISSN 0195-6108.

9. BORKOWSKI, K., KŁODOWSKI, K., FIGIEL, H., KRZYŻAK, A. T. A theoretical validation of the B-matrix spatial distribution approach to diffusion tensor imaging. *Magnetic Resonance Imaging*. 2017, **36**(February), 1-6. ISSN 0730-725X. DOI: 10.1016/j.mri.2016.10.002.

10. BORKOWSKI, K., KRZYŻAK, A. T. Analysis and correction of errors in DTI-based tractography due to diffusion gradient inhomogeneity. *Journal of Magnetic Resonance*. 2018, **296**(November), 5-11. ISSN 1090-7807. DOI: 10.1016/j.jmr.2018.08.011.

11. BREIER, A., BUCHANAN, R. W., ELKASHEF, A., MUNSON, R. C., KIRKPATRICK, B., GELLAD, F. Brain morphology and schizophrenia. A magnetic resonance imaging study of limbic, prefrontal cortex, and caudate structures. *Archives of General Psychiatry.* 1992, **49**(12), 921-926. ISSN 0003-990X. DOI: 10.1001/archpsyc.1992.01820120009003.

12. BRUGGER, S. P., HOWES, O. D. Heterogeneity and homogeneity of regional brain structure in schizophrenia: A meta-analysis. *JAMA Psychiatry.* 2017, **74**(11), 1104-1111. ISSN 2168-622X. DOI: 10.1001/jamapsychiatry.2017.2663.

13. CACHIA, A., BORST, G., TISSIER, C., FISHER, C., PLAZE, M., GAY, O., RIVIERE, D., GOGTAY, N., GIEDD, J., MANGIN, J. F., HOUDE, O., RAZNAHAN, A. Longitudinal stability of the folding pattern of the anterior cingulate cortex during

development. *Developmental Cognitive Neuroscience*. 2016, **19**(June), 122-127. ISSN 1878-9293. DOI: 10.1016/j.dcn.2016.02.011.

14. CHANDARANA, H., WANG, H., TIJSSEN, R. H. N., DAS, I. J. Emerging role of MRI in radiation therapy. *Journal of Magnetic Resonance Imaging*. 2018, **48**(6), 1468-1478. ISSN 1053-1807. DOI: 10.1002/jmri.26271.

15. CROSSLEY, N. A., ALLIENDE, L. M., CZEPIELEWSKI, L. S., ACEITUNO, D., CASTAÑEDA, C. P., DIAZ, C., IRURETAGOYENA, B., MENA, C., MENA, C., RAMIREZ-MAHALUF, J. P., TEPPER, A., VASQUEZ, J., FONSECA, L., MACHADO, V., HERNÁNDEZ, C. E., VARGAS-UPEGUI, C., GOMEZ-CRUZ, G., KOBAYASHI-ROMERO, L. F., MONCADA-HABIB, T., ARANGO, C., BARCH, D. M., CARTER, C., CORRELL, C. U., FREIMER, N. B., MCGUIRE, P., EVANS-LACKO, S., UNDURRAGA, E., BRESSAN, R., GAMA, C. S., LOPEZ-JARAMILLO, C., DE LA FUENTE-SANDOVAL, C., GONZALEZ-VALDERRAMA, A., UNDURRAGA, J., GADELHA, A. The enduring gap in educational attainment in schizophrenia according to the past 50 years of published research: a systematic review and meta-analysis. *Lancet Psychiatry*. 2022, **9**(7), 565-573. ISSN 2215-0366. DOI: 10.1016/S2215-0366(22)00121-3.

16. CRUZ-ORIVE, L. Stereology: a historical survey. *Image Analysis & Stereology*. 2017, **36**(3), 153-177. ISSN 1580-3139. DOI: https://doi.org/10.5566/ias.1767.

17. DE CASTRO, F. Cajal and the Spanish Neurological School: Neuroscience Would Have Been a Different Story Without Them. 2019. *Frontiers in Cellular Neuroscience*. 2019, **24**(13), 187. ISSN 1662-5102. DOI: 10.3389/fncel.2019.00187.

18. DEEB, W., SALVATO, B., ALMEIDA, L., FOOTE, K. D., AMARAL, R., GERMANN, J., ROSENBERG, P. B., TAN-WAI, D. F., WOLK, D. A., BURKE, A. D., SALLOWAY, S., SABBAGH, M. N., CHAKRAVARTY, M. M., SMITH, G. S., LYKETSOS, C. G., LOZANO, A. M., OKUN, M. S. Fornix-Region Deep Brain Stimulation-Induced Memory Flashbacks in Alzheimer's Disease. *New England Journal of Medicine*. 2019, **381**(8), 783-785. ISSN 0028-4793. DOI: 10.1056/NEJMc1905240.

19. DELONG, M. R., WICHMANN, T. Circuits and circuit disorders of the basal ganglia. *Archives of Neurology*. 2007, **64**(1), 20-24. ISSN 0003-9942. DOI: 10.1001/archneur.64.1.20.

20. DELVECCHIO, G., PIGONI, A., PERLINI, C., BARILLARI, M., VERSACE, A., RUGGERI, M., ALTAMURA, A. C., BELLANI, M., BRAMBILLA, P. A diffusion weighted imaging study of basal ganglia in schizophrenia. *International Journal of Psychiatry in Clinical Practice*. 2018, **22**(1), 6-12. ISSN 1365-1501. DOI: 10.1080/13651501.2017.1340650.

21. DESTRIEUX, C., TERRIER, L. M., ANDERSSON, F., LOVE, S. A., COTTIER, J.P., DUVERNOY, H., VELUT, S., JANOT, K., ZEMMOURA, I. Practical guide for the identification of major sulcogyral structures of the human cortex. *Brain Struct. Funct*. 2017 **222**. 2001-2015. DOI: 10.1007/s00429-016-1320-z

22. DUAN, M., CHEN, X., HE, H., JIANG, Y., JIANG, S., XIE, Q., LAI, Y., LUO, C., YAO, D. Altered Basal Ganglia Network Integration in Schizophrenia. *Frontiers in Human Neuroscience*. 2015, **9**(October), 561. ISSN 662-5161. DOI: 10.3389/fnhum.2015.00561.

23. ELIAS, H. Address of the president. In: HAUG, H., ed. *Proceedings of the 1st International Congress for Stereology*. Wien: Congressprint, 1963.

24. ESTÉVEZ-SANTÉ, S., JIMÉNEZ-HUETE, A. Comparative analysis of methods of volume adjustment in hippocampal volumetry for the diagnosis of Alzheimer disease. *Journal of Neuroradiology*. 2020, **47**(2), 161-165. ISSN 0150-9861. DOI: 10.1016/j.neurad.2019.02.004.

25. FENG, N., PALANIYAPPAN, L., ROBBINS, T. W., CAO, L., FANG, S., LUO, X., WANG, X., LUO, Q. Working memory processing deficit associated with a nonlinear response pattern of the anterior cingulate cortex in first-episode and drug-naïve schizophrenia. *Neuropsychopharmacology.* 2023, **48**(3), 552-559. ISSN 0893-133X. DOI: 10.1038/s41386-022-01499-8.

26. FIPAT. *Terminologia Neuroanatomica* [online]. 2017. Dostupné z: https://fipat.library.dal.ca/TNA.

27. FORNITO, A., WOOD, S. J., WHITTLE, S., FULLER, J., ADAMSON, C., SALING, M. M., VELAKOULIS, D., PANTELIS, C., YÜCEL, M. Variability of the paracingulate sulcus and morphometry of the medial frontal cortex: associations with cortical thickness, surface area, volume, and sulcal depth. *Human Brain Mapping*. 2008, **29**(2), 222-236. ISSN 1065-9471. DOI: 10.1002/hbm.20381.

28. FORNITO, A., YUCEL, M., DEAN, B., WOOD, S.J., PANTELIS C. Anatomical abnormalities of the anterior cingulate cortex in schizophrenia: Bridging the gap between neuroimaging and neuropathology. *Schizophrenia Bulletin.* 2009, **35**(5), 973-993. ISSN 0586-7614. DOI: 10.1093/schbul/sbn025.

29. FRITZSCHE KH, LAUN FB, MEINZER HP, STIELTJES B. Opportunities and pitfalls in the quantification of fiber integrity: what can we gain from Q-ball imaging? *Neuroimage.* 2010 ,**51**(1):242-51. DOI: 10.1016/j.neuroimage.2010.02.007.

30. FUNG, Y. L., NG, K. E. T., VOGRIN, S. J., MEADE, C., NGO, M., COLLINS, S. J., BOWDEN, S. C. Comparative utility of manual versus automated segmentation of hippocampus and entorhinal cortex volumes in a memory clinic sample. *Journal of Alzheimer's Disease.* 2019, **68**(1), 159-171. ISSN 1387-2877. DOI: 10.3233/JAD-181172.

31. GARRISON, J. *Paracingulate Sulcus Measurement Protocol*. Cambridge: University of Cambridge, 2017.

32. GARRISON, J. R., FERNYHOUGH, C., MCCARTHY-JONES, S., HAGGARD, M., SIMONS, J. S. Paracingulate sulcus morphology is associated with hallucinations in the human brain. *Nature Communications*. 2015, **6**(November), 8956. ISSN 2041-1723. DOI: 10.1038/ncomms9956.

33. GARRISON, J. R., FERNYHOUGH, C., MCCARTHY-JONES, S., SIMONS, J. S., AND SOMMER, I. E. C. Paracingulate Sulcus Morphology and Hallucinations in Clinical and Nonclinical Groups. *Schizophrenia Bulletin*. 2019, **45**(4), 733-741. ISSN 0586-7614. DOI: 10.1093/schbul/sby157.

34. GE, T., CHEN, C. Y., DOYLE, A. E., VETTERMANN, R., TUOMINEN, L. J., HOLT, D. J., SABUNCU, M. R., SMOLLER, J. W. The Shared Genetic Basis of

Educational Attainment and Cerebral Cortical Morphology. *Cereberal Cortex*. 2019, **29**(8), 3471-3481. ISSN 1047-3211. DOI: 10.1093/cercor/bhy216.

35. GEROLDI, C., AKKAWI, N. M., GALLUZZI, S., UBEZIO, M., BINETTI, G., ZANETTI, O, TRABUCCHI, M, FRISONI, G. B. Temporal lobe asymmetry in patients with Alzheimer's disease with delusions. *Journal of Neurology, Neurosurgery and Psychiatry.* 2000, **69**(2), 187-191. ISSN 0022-3050. SOI: 10.1136/jnnp.69.2.187.

36. GESCHWIND, N. Disconnexion syndromes in animals and man. I. *Brain.* 1965, **88**(2), 237-294. ISSN 0006-8950. DOI: 10.1093/brain/88.2.237

37. GHAI, S., FONG, K. W., TOI, A., CHITAYAT, D., PANTAZI, S., BLASER, S. Prenatal US and MR imaging findings of lissencephaly: review of fetal cerebral sulcal development. *Radiographics*. 2006, **26**(2), 389-405. ISSN 0271-5333. DOI: 10.1148/rg.262055059.

38. GIESEL, F. L., HAHN, H. K., THOMANN, P. A., WIDJAJA, E., WIGNALL, E., VON TENGG-KOBLIGK, H., PANTEL, J., GRIFFITHS, P. D., PEITGEN, H. O., SCHRODER, J., ESSIG, M. Temporal horn index and volume of medial temporal lobe atrophy using a new semiautomated method for rapid and precise assessment. AJNR. *American Journal of Neuroradiology.* 2006, **27**(7), 1454-1458. ISSN 0195-6108.

39. GOOD, C. D., JOHNSRUDE, I. S., ASHBURNER, J., HENSON, R. N. A., FRISTON, K. J., FRACKOWIAK, R. S. J. Cerebral asymmetry and the effects of sex and handedness on brain structure: A voxel-based morphometric analysis of 465 normal adult human brains. *NeuroImage*. 2001, **14**(3), 685-700. ISSN 1053-8119. DOI:10.1006/nimg.2001.0857.

40. GRADY, C. L., MCINTOSH, A. R., BEIG, S., KEIGHTLEY, M. L., BURIAN, H., BLACK, S. E. Evidence from functional neuroimaging of a compensatory prefrontal network in Alzheimer's disease. *Journal of Neuroscience.* 2003, **23**(3), 986-993. ISSN 0270-6474. DOI: 10.1523/JNEUROSCI.23-03-00986.2003.

41. GRILLNER, S., ROBERTSON, B. The Basal Ganglia Over 500 Million Years. *Current Biology*. 2016, **26**(20), R1088-R1100. ISSN 0960-9822. DOI: 10.1016/j.cub.2016.06.041.

42. GROTHE, M. J., BARTHEL, H., SEPULCRE, J., DYRBA, M., SABRI, O., TEIPEL, S. J. In vivo staging of regional amyloid deposition. *Neurology.* 2017, **89**(20), 2031-2038. ISSN 0028-3878. DOI: 10.1212/WNL.0000000000004643.

43. GUILLERY, R. W. Observations of synaptic structures: origins of the neuron doctrine and its current status. *Philosophical Transactions of the Royal Society of London. Series B, Biological Sciences.* 2005, **360**(1458), 1281-1307. ISSN 0962-8436. DOI: 10.1098/rstb.2003.1459.

44. HARI, E., KURT, E., BAYRAM, A., KIZILATES-EVIN, G., ACAR, B., DEMIRALP, T., GURVIT, H. Volumetric changes within hippocampal subfields in Alzheimer's disease continuum. *Neurological Sciences*. 2022, **43**(7), 4175-4183. ISSN 1590-1874. DOI:10.1007/s10072-022-05890-7.

45. HARPER, L., BARKHOF, F., FOX, N. C., SCHOTT, J. M. Using visual rating to diagnose dementia: a critical evaluation of MRI atrophy scales. *Journal of Neurology, Neurosurgery and Psychiatry.* 2015, **86**(11), 1225-1233. ISSN 0022-3050. DOI: 10.1136/jnnp-2014-310090.

46. HAUG, H. History of neuromorphometry. *Journal of Neuroscience Methods.* 1986, **18**(1-2), 1-17. ISSN 0165-0270. DOI: 10.1016/0165-0270(86)90110-x.

47. HECKERS, S. Neuroimaging studies of the hippocampus in schizophrenia. *Hippocampus*. 2001, **11**(5), 520-528. ISSN 1050-9631. DOI: 10.1002/hipo.1068.

48. HORSKÁ, A., BARKER, P. B. Imaging of brain tumors: MR spectroscopy and metabolic imaging. *Neuroimaging Clinics of North America.* 2010, **20**(3), 293-310. ISSN 1052-5149. DOI: 10.1016/j.nic.2010.04.003.

49. HU, X., MEIBERTH, D., NEWPORT, B., JESSEN, F. Anatomical correlates of the neuropsychiatric symptoms in Alzheimer's disease. *Current Alzheimer Research*. 2015, **12**(3), 266-277. ISSN 1567-2050. DOI: 10.2174/1567205012666150302154914.

50. JACKSON, S. R., PARKINSON, A., JUNG, J., RYAN, S. E., MORGAN, P. S., HOLLIS, C., JACKSON, G. M. Compensatory neural reorganization in Tourette syndrome. *Current Biology*. 2011, **21**(7), 580-585. ISSN 0960-9822. DOI: 10.1016/j.cub.2011.02.047.

51. JAHNG, G.-H., PARK, S., RYU, C.-W., CHO, Z.-H. Magnetic Resonance Imaging: Historical Overview, Technical Developments, and Clinical Applications *Progress in Medical Physics.* 2020, **31**(3), 35-53. ISSN 2508-4453. DOI: 10.14316/pmp.2020.31.3.35.

52. JI, E., GUEVARA, P., GUEVARA, M., GRIGIS, A., LABRA, N., SARRAZIN, S., HAMDANI, N., BELLIVIER, F., DELAVEST, M., LEBOYER, M., TAMOUZA, R., POUPON, C., MANGIN, J.-F., HOUENOU, J. Increased and Decreased Superficial White Matter Structural Connectivity in Schizophrenia and Bipolar Disorder. *Schizophrenia Bulletin*. 2019, **45**(6), 1367–1378. ISSN 0586-7614. DOI: 10.1093/schbul/sbz015.

53. JONES, D. K., CERCIGNANI, M. Twenty-five Pitfalls in the Analysis of Diffusion MRI Data. *NMR in Biomedicine*. 2010, **23**(7), 803-820. ISSN 0952-3480. DOI: 10.1002/nbm.1543.

54. KAWAHARA, D., NAGANA, Y. T1-weighted and T2-weighted MRI image synthesis with convolutional generative adversarial networks. *Reports of Practical Oncology and Radiotherapy.* 2021, **26**(1), 35-42. ISSN 1507-1367. DOI: 10.5603/RPOR.a2021.0005.

55. KILIMANN, I., GROTHE, M., HEINSEN, H., ALHO, E. J., GRINBERG, L., AMARO, E., DOS SANTOS, G. A., DA SILVA, R. E., MITCHELL, A. J., FRISONI, G.B., BOKDE, A. L. W., FELLGIEBEL, A., FILIPPI, M., HAMPEL, H., KLÖPPEL, S., TEIPEL, S. J. Subregional basal forebrain atrophy in Alzheimer's disease: A multicenter study. *Journal of Alzheimer's Disease*. 2014, **40**(3), 687-700. ISSN 1387-2877. DOI: 10.3233/JAD-132345.

56. KLASSON, N., OLSSON, E., ECKERSTRÖM, C., MALMGREN, H., WALLIN, A. Estimated intracranial volume from FreeSurfer is biased by total brain volume. *European*

Radiology Experimental. 2018, **2**(September), 24. (a) ISSN 2509-9280. DOI: 10.1186/s41747-018-0055-4.

57. KLASSON, N., OLSSON, E., ECKERSTRÖM, C., MALMGREN, H., WALLIN, A. Delineation of two intracranial areas and the perpendicular intracranial width is sufficient for intracranial volume estimation. *Insights into Imaging.* 2018, **9**(1), 25-34.(b) ISSN 1869-4101. DOI:10.1007/s13244-017-0583-0.

58. KUBICKI, M., MCCARLEY, R. W., SHENTON, M. E. Evidence for white matter abnormalities in schizophrenia. *Current Opinion in Psychiatry.* 2005, **18**(2), 121-134. ISSN 0951-7367. DOI: 10.1097/00001504-200503000-00004.

59. KUCHTOVÁ, B., WURST, Z., MRZÍLKOVÁ, J., IBRAHIM, I., TINTĚRA, J., BARTOŠ, A., MUSIL, V., KIESLICH, K., ZACH, P. Compensatory Shift of Subcallosal Area and Paraterminal Gyrus White Matter Parameters on DTI in Patients with Alzheimer Disease. *Current Alzheimer Research*. 2018, **15**(6), 590-599. ISSN 1567-2050. DOI: 10.2174/1567205015666171227155510.

60. KUTOVÁ, M., MRZÍLKOVÁ, J., KIRDAJOVÁ, D, ŘÍPOVÁ, D., ZACH, P. Simple method for evaluation of planum temporale pyramidal neurons shrinkage in postmortem tissue of Alzheimer disease patients. *BioMed Research International*. 2014, (February), 607171. ISSN 2314-6133. DOI: 10.1155/2014/607171.

61. KUTOVÁ, M., MRZÍLKOVÁ, J., RIEDLOVÁ, J., ZACH, P. Asymmetric Changes in Limbic Cortex and Planum Temporale in Patients with Alzheimer Disease. *Current Alzheimer Research*. 2018, **15**(14), 1361-1368. ISSN 1567-2050. DOI: doi:10.2174/1567205015666181004142659.

62. LAKSHMISHA RAO, Y. L., GANARAJA, B., MURLIMANJU, B. V., JOY, T., KRISHNAMURTHY, A., AGRAWAL, A. Hippocampus and its involvement in Alzheimer's disease: a review. *3 Biotech*. 2022, **12**(2), 55. ISSN 2190-572X. DOI: 10.1007/s13205-022-03123-4.

63. LANGHAMMER, C. G., PREVITERA, M. L., SWEET, E. S., SRAN, S. S., CHEN, M., FIRESTEIN, B. L. Automated Sholl analysis of digitized neuronal morphology at multiple scales: Whole cell Sholl analysis versus Sholl analysis of arbor subregions. *Cytometry A*. 2010, **77**(12), 1160-1168. ISSN 1552-4922. DOI: 10.1002/cyto.a.20954.

64. LE PROVOST, J. B., BARTRES-FAZ, D., PAILLERE-MARTINOT, M. L., ARTIGES, E., PAPPATA, S., RECASENS, C., PEREZ-GOMEZ, M., BERNARDO, M., BAEZA, I., BAYLE, F., MARTINOT, J. L. Paracingulate sulcus morphology in men with early-onset schizophrenia. *British Journal of Psychiatry.* 2003, **182**, 228-232. ISSN 0007-1250. DOI: 10.1192/bjp.182.3.228.

65. LI F, TAKECHI H, SAITO R, AYAKI T, KOKURYU A, KUZUYA A, TAKAHASHI R. A comparative study: visual rating scores and the voxel-based specific regional analysis system for Alzheimer's disease on magnetic resonance imaging among subjects with Alzheimer's disease, mild cognitive impairment, and normal cognition. *Psychogeriatrics*. 2019, **19**(2), 95-104, DOI: 10.1111/psyg.12370.

66. LI, Q., YAO, L., YOU, W., LIU, J., DENG, S., LI, B., LUO, L., ZHAO, Y., WANG, Y., ZHANG, Q., LONG, F., SWEENEY, J. A., GU, S., LI, F., GONG, Q. Controllability

of Functional Brain Networks and Its Clinical Significance in First-Episode Schizophrenia. *Schizophrenia Bulletin*. 2023, **49**(3), 659-668. ISSN 0586-7614. DOI: 10.1093/schbul/sbac177.

67. LIU IC, CHIU CH, CHEN CJ, KUO LW, LO YC, TSENG WY. The microstructural integrity of the corpus callosum and associated impulsivity in alcohol dependence: a tractography-based segmentation study using diffusion spectrum imaging. *Psychiatry Res.* 2010,**184**(2),128-34. DOI: 10.1016/j.pscychresns.2010.07.002.

68. MACDONALD, K. E., BARTLETT, J. W., LEUNG, K. K., OURSELIN, S., BARNES, J. The value of hippocampal and temporal horn volumes and rates of change in predicting future conversion to AD. *Alzheimer Disease and Associated Disorders*. 2013, **27**(2), 168-173. ISSN 0893-0341. DOI: 10.1097/WAD.0b013e318260a79a.

69. MAHON, P. B., ELDRIDGE, H., CROCKER, B., NOTES, L., GINDES, H., POSTELL, E., KING, S., POTASH, J. B., RATNANATHER, J. T., BARTA, P. E. An MRI study of amygdala in schizophrenia and psychotic bipolar disorder. *Schizophrenia Research*. 2012, **138**(2-3), 188-191. ISSN 0920-9964. DOI: 10.1016/j.schres.2012.04.005.

70. MAINA, J. N. 5. Application of Morphometric and Stereological Techniques on Analysis and Modelling of the Avian Lung. In: PARES-CASANOVA, P. M., ed. *New Insights into Morphometry Studies*. InTech, 2017. ISBN 978-953-51-3365-0. DOI: 10.5772/intechopen.69062.

71. MARINESCU, I., MELINTE, P. R., DINCĂ, I., PĂTRASCU, E., BOTORAN MEŞINĂ, M. I., DRĂGOI, G. S. Human gyrus cinguli as an anatomic marker in the neuronal system processing behavioural and cognitive act. Implications in forensic psychopathology. *Romanian Journal of Legal Medicine*. 2018, **26**(1), 1-11. ISSN 1221-8618. DOI: 10.4323/rjlm.2018.1.

72. MCGRATH, J., SAHA, S., CHANT, D., WELHAM, J. Schizophrenia: a concise overview of incidence, prevalence, and mortality. *Epidemiologic Reviews*. 2008, **30**(1), 67-76. ISSN 0193-936X. DOI: 10.1093/epirev/mxn001.

73. MCKHANN, G. M., KNOPMAN, D. S., CHERTKOW, H., HYMAN, B. T., JACK, C. R., KAWAS, C. H., KLUNK, W. E., KOROSHETZ, W. J., MANLY, J. J., MAYEUX, R., MOHS, R. C., MORRIS, J. C., ROSSOR, M. N., SCHELTENS, P., CARRILLO, M. C., ZHIES, B., WEINTRAUB, S., PHELPS, C. H. The diagnosis of dementia due to Alzheimer's disease: Recommendations from the National Institute on Aging-Alzheimer's Association workgroups on diagnostic guidelines for Alzheimer's disease. *Alzheimer's & Dementia*. 2011, **7**(3), 263-269. ISSN 1552-5260. DOI: 10.1016/j.jalz.2011.03.005.

74. MENENDEZ-GONZALEZ M, LOPEZ-MUNIZ A, VEGA JA, SALAS-PACHEHO JM, ARIAS-CARRION O. MTA index: a simple 2D-method for assessing atrophy of the medial temporal lobe using clinically available neuroimaging. *Front Aging Neurosci.* 2014, **6**(23), 1-6. ISSN 1663-4365. DOI: 10.3389/fnagi.2014.00023

75. MENG, Y., LI, G., WANG, L., LIN, W., GILMORE, J. H., SHEN, D. Discovering cortical sulcal folding patterns in neonates using large-scale dataset. *Human Brain Mapping*. 2018, **39**(9), 3625-3635. ISSN 1065-9471. DOI: 10.1002/hbm.24199.

76. NISHIKUNI, K., RIBASI, G. C. Study of fetal and postnatal morphological development of the brain sulci. *Journal of Neurosurgery. Pediatrics*. 2013, **11**(1), 1-11. ISSN 1933-0707. DOI: 10.3171/2012.9.PEDS12122.

77. NOGA, J. T., AYLWARD, E., BARTA, P. E., PEARLSON, G. C. Cingulate gyrus in schizophrenic patients and normal volunteers. *Psychiatry Research.* 1995, **61**(4), 201-208. ISSN 0165-1781. DOI: 10.1016/0925-4927(95)02612-2.

78. ONO, M., KUBIK, S., ABARNATHEY, C. D. *Atlas of the Cerebral Sulci.* New York: Georg Thieme, 1990.

79. ORBAN, P., DESSEILLES, M., MENDREK, A., BOURQUE, J., BELLEC, P., STIP, E. Altered brain connectivity in patients with schizophrenia is consistent across co gnitive contexts. *Journal of Psychiatry & Neuroscience*. 2017, **42**(1), 17-26. ISSN 1180-4882. DOI: 10.1503/jpn.150247.

80. ORTH, D. *Essentials of radiologic science*. Praha: Wolters Kluwer ČR, 2012. ISBN 978-14-9631-727-8.

81. PASI M, VAN UDEN IW, TULADHAR AM, DE LEEUW FE, PANTONI L. WHITE Matter Microstructural Damage on Diffusion Tensor Imaging in Cerebral Small Vessel Disease: Clinical Consequences. *Stroke*. 2016, **47**(6),1679-84. DOI:10.1161/STROKEAHA.115.012065.

82. PASQUINI, J., DURCAN, R., WIBLIN, L., GERSEL STOKHOLM, M., ROCHESTER, L., BROOKS, D. J., BURN, D., PAVESE, N. Clinical implications of early caudate dysfunction in Parkinson's disease. *Journal of Neurology, Neurosurgery, and Psychiatry*. 2019, **90**(10), 1098-1104. ISSN 0022-3050. DOI: 10.1136/jnnp-2018-320157.

83. PAUS, T., TOMAIUOLO, F., OTAKY, N., MACDONALD, D., PETRIDES, M., ATLAS, J., MORRIS, R., EVANS, A. C. Human cingulate and paracingulate sulci: Pattern, variability, asymmetry, and probabilistic map. *Cerebral Cortex.* 1996, **6**(2), 207-214. ISSN 1047-3211. DOI: 10.1093/cercor/6.2.207.

84. PERL, D. P. Neuropathology of Alzheimer's disease. *Mount Sinai Journal of Medicine*. 2010, **77**(1), 32-42. ISSN 0027-2507. DOI: 10.1002/msj.20157.

85. PORTER, B. S., SCHMIDT, R., BILKEY, D. K. Hippocampal place cell encoding of sloping terrain. *Hippocampus.* 2018, **28**(11), 767-782. ISSN 1050-9631. DOI: 10.1002/hipo.22966.

86. RAMETTI, G., JUNQUE, C., BARTRES-FAZ, D., ZUBIAURRE-ELORZA, L., CATALAN, R., PENADES, R., BARGALLO, N., BERNARDO, M. Anterior cingulate and paracingulate sulci morphology in patients with schizophrenia. *Schizophrenia Research.* 2010, **121**(1-3), 66-74. ISSN 0920-9964. DOI: 10.1016/j.schres.2010.05.016.

87. RAMON Y CAJAL, S. *Textura Del Sistema Nervioso Del Hombre y De Los Vertebrados: Estudios Sobre El Plan Estructural y Composición Histológica De Los Centros Nerviosos Adicionados De Consideraciones Fisiológicas Fundadas En Los Nuevos Descubrimientos*. Madrid: N. Moya, 1852-1934.

88. RUSHWORTH, M. F. S., WALTON, M. E., KENNERLEY, S. W., BANNERMANN, D. M. Action sets and decisions in the medial frontal cortex. *Trends in Cognitive Sciences*. 2004, **8**(9), 410-417. ISSN 1364-6613. DOI: 10.1016/j.tics.2004.07.009.

89. SALK, I., ATALAR, M. H., SEZER, F., EGILMEZ, H., CETIN, A., ARSLAN, M. An MRI study of age-related changes in the dimensions related temporal lobe. *International Journal of Clinical and Experimental Medicine.* 2014, **7**(3), 515-522. ISSN 1940-5901.

90. SANJARI MOGHADDAM, H., DOLATSHAHI, M., MOHEBI, F., AARABI, M. H. Structural white matter alterations as compensatory mechanisms in Parkinson's disease: A systematic review of diffusion tensor imaging studies. *Journal of Neuroscience Research*. 2020, **98**(7), 1398-1416. ISSN 0360-4012. DOI: 10.1002/jnr.24617.

91. SCHOEMAKER, D., BUSS, C., PIETRANTONIO, S., MAUNDER, L., DAWN FREIESLEBEN, S., HARTMANN, J., LOUIS COLLINS, D., LUPIEN, S., PRUESSNER, J. C. The hippocampal-to-ventricle ratio (HVR): presentation of a manual segmentation protocol and preliminary evidence. *Neuroimage.* 2019, **203**(December), 116108. ISSN 1053-8119. DOI: 10.1016/j.neuroimage.2019.

92. SHENTON, M. E., WHITFORD, T. J., KUBICKI, M. Structural neuroimaging in schizophrenia: from methods to insights to treatments. *Dialogues in Clinical Neuroscience.* 2010, **12**(3), 317-332. ISSN 1294-8322. DOI: 10.31887/DCNS.2010.12.3/mshenton.

93. SHI, F., LIU, B., ZHOU, Y., YU, C., JIANG, T. Hippocampal volume and asymmetry in mild cognitive impairment and Alzheimer's disease: Meta-analyses of MRI studies. *Hippocampus*. 2009, **19**(11), 1055-1064. ISSN 1050-9631. DOI: 10.1002/hipo.20573.

94. SMITH, G. E. A New Topographical Survey of the Human Cerebral Cortex, being an Account of the Distribution of the Anatomically Distinct Cortical Areas and their Relationship to the Cerebral Sulci. *Journal of Anatomy and Physiology.* 1907, **41**(Pt. 4), 237-254.

95. SØRENSEN, L., IGEL, C., LIV HANSEN, N., OSLER, M., LAURITZEN, M., ROSTRUP, E., NIELSEN, M. Early detection of Alzheimer's disease using MRI hippocampal texture. *Human Brain Mapping*. 2016, **37**(3), 1148-1161. ISSN 1065-9471. DOI: 10.1002/hbm.23091.

96. SUN, Z.Y., PERROT, M., TUCHOLKA, A., RIVIERE, D., MANGIN, J. F. Constructing a dictionary of human brain folding patterns. *Medical Image Computing and Computer-Assisted Intervention*. 2009, **12**(Pt. 2), 117-124. ISSN 0302-9743. DOI: 10.1007/978-3-642-04271-3_15.

97. TAKASHIMA, A., PETERSSON, K. M., RUTTERS, F., TENDOLKAR, I., JENSEN, O., ZWARTS, M. J., MCNAUGHTON, B. L., FERNÁNDEZ, G. Declarative memory consolidation in humans: a prospective functional magnetic resonance imaging study. *Proceedings of the National Academy of Sciences of the United States of America*. 2006, **103**(3), 756-761. ISSN 0027-8424. DOI: 10.1073/pnas.0507774103.

98. TANG, Y., LUTZ, M.W., XING, Y. A systems-based model of Alzheimer's disease. *Alzheimer's & Dementia.* 2019, **15**(1), 168-171. ISSN 1552-5260. DOI: 10.1016/j.jalz.2018.06.3058.

99. THOMPSON P. M., HAYASHI K. M., DE ZUBICARAY G. I., JANKE, A. L., ROSE, S. E., SEMPLE, J., HONG, M. S., HERMAN, D. H., GRAVANO, D., DODDREL, D. M., TOGA, A. W. Mapping hippocampal and ventricular change in Alzheimer disease. *NeuroImage.* 2004, **22**(4), 1754-1766. ISSN 1053-8119. DOI: 10.1016/j.neuroimage.2004.03.040.

100. TOGA, A. W., THOMPSON, P. M. Mapping brain asymmetry. *Nature Reviews. Neuroscience*. 2003, **4**(1), 37-48. ISSN 1471-003X. DOI: 10.1038/nrn1009.

101. TUCHOLKA, A., GRAU-RIVERA, O., FALCON, C., RAMI, L., SANCHEZ-VALLE, R., LLADO, A., GISPERT, J. D., MOLINUEVO, J. L. Structural Connectivity Alterations Along the Alzheimer's Disease Continuum: Reproducibility Across Two Independent Samples and Correlation with Cerebrospinal Fluid Amyloid-beta and Tau. *Journal of Alzheimer's Disease*. 2018, **61**(4), 1575-1587. ISSN 1387-2877. DOI: 10.3233/JAD-170553.

102. TULADHAR, A. M., REID, A. T., SHUMSKAYA, E., DE LAAT, K. F., VAN NORDEN, A. G. W., VAN DIJK, E. J., NORRIS, D. G., DE LEEUW, F. E. Relationship between white matter hyperintensities, cortical thickness, and cognition. *Stroke*. 2015, **46**(2), 425-432. ISSN 0039-2499. DOI: 10.1161/STROKEAHA.114.007146.

103. VAN ERP, T. G., HIBAR, D. P., RASMUSSEN, J. M., GLAHN, D. C., PEARLSON, G. D., ANDREASSEN O. A., et al. 2016. Subcortical brain volume abnormalities in 2028 individuals with schizophrenia and 2540 healthy controls via the ENIGMA consortium. *Molecular Psychiatry.*2016, **21**(4), 547-553. ISSN 1359-4184. DOI: 10.1038/mp.2015.63.

104. VITÁ, A., SACCHETTI, E., CALZERONI, A., CAZZULLO, L. C. Cortical atrophy in schizophrenia. Prevalence and associated features. *Schizophrenia Research*. 1988, **1**(5), 329-337. ISSN 0920-9964. DOI: 10.1016/0920-9964(88)90046-1.

105. WEI, X., YIN, Y., RONG, M., ZHANG, J., WANG, L., WU, Y., CAI, Q., YU, C., WANG, J., JIANG, T. Paracingulate Sulcus Asymmetry in the Human Brain: Effects of Sex, Handedness, and Race. *Scientific Reports.* 2017, **7**(February), 42033. ISSN 2045-2322. DOI: 10.1038/srep42033.

106. WEINBERGER, D. R., MARENCO, S. Schizophrenia as A Neurodevelopmental Disorder. In: HIRSCH, S. R. W., ed. *Schizophrenia.* 2nd ed. London: Blackwell Publishing, 2003, s. 326-348.

107. WOODS, B. T. Is schizophrenia a progressive neurodevelopmental disorder? Toward a unitary pathogenetic mechanism. *American Journal of Psychiatry*. 1998, **155**(12), 1661-1670. ISSN 0002-953X. DOI: 10.1176/ajp.155.12.1661.

108. WRIGHT, N., ALHINDI, A., MILLIKIN, C., MODIRROUSTA, M., UDOW, S., BORYS, A., ANANG, J., HOBSON, D. E., KO, J. H. Elevated caudate connectivity in cognitively normal Parkinson's disease patients. *Scientific Reports*. 2020, **10**(October), 17978. ISSN 2045-2322. DOI: 10.1038/s41598-020-75008-6.

109. XEKARDAKI, A., GIANNAKOPOULOS, P., HALLER, S. White Matter Changes in Bipolar Disorder, Alzheimer Disease, and Mild Cognitive Impairment: New Insights from DTI. *Journal of Aging Research*. 2011, **2011**(December), 286564. ISSN 2090-2204. DOI: 10.4061/2011/286564.

110. YEH, F. C., VERSTYNEN, T. D., WANG, Y., FERNANDEZ-MIRANDA, J. C., TSENG, W. Y. Deterministic diffusion fiber tracking improved by quantitative anisotropy. *PLoS One*. 2013, **8**(11), e80713. ISSN 1932-6203. DOI: 10.1371/journal.pone.0080713.

111. YÜCEL, M., STUART, G. W., MARUFF, P., VELAKOULIS, D., CROWE, S.F., SAVAGE, G., PANTELIS, C. Hemispheric and gender-related differences in the gross morphology of the anterior cingulate/paracingulate cortex in normal volunteers: An MRI morphometric study. *Cerebral Cortex*. 2001, **11**(1), 17-25. ISSN 1047-3211. DOI: 10.1093/cercor/11.1.17.

112. ZACH, P., KRIŠTOFIKOVÁ, Z., MRZÍLKOVÁ, J., MAJER, E., SELINGER, P., SPANIEL, F., ŘÍPOVÁ, D., KENNEY, J. Planum temporale analysis via a new volumetric method in autoptic brains of demented and psychotic patients. *Current Alzheimer Research*. 2009, **6**(1), 69-76. ISSN 1567-2050. DOI: 10.2174/156720509787313907.

113. ZACH, P., MRZÍLKOVÁ, J., ŘEZÁČOVÁ, L., STUCHLÍK, A., VALEŠ, K. Delayed effects of elevated corticosterone level on volume of hippocampal formation in laboratory rat. *Physiological Research*. 2010, **59**(6), 985-996. ISSN 0862-8408. DOI: 10.33549/physiolres.931904.

114. ZHANG, H., WANG, Y., LU, T., QIU, B., TANG, Y., OU, S., TIE, X., SUN, C., XU, K. Differences between generalized q-sampling imaging and diffusion tensor imaging in the preoperative visualization of the nerve fiber tracts within peritumoral edema in the brain. *Neurosurgery*. 2013, **73**(6), 1044-1053. ISSN 0148-396X. DOI: 10.1227/NEU.0000000000000146.

115. ZHANG, X., LI, Y., GUAN, Q., DONG, D., ZHANG, J., MENG, X., CHEN, F., LUO, Y., ZHANG, H. Distance-dependent reconfiguration of hubs in Alzheimer's disease: a cross-tissue functional network study. *bioRxiv* [Preprint]. 2023. DOI: 10.1101/2023.03.24.532772.

9. Publications *in extenso*, which are the basis of the dissertation

First author

1. **LAHUTSINA, Anastasiya**; ŠPANIEL, Filip; MRZÍLKOVÁ, Jana; MOROZOVA, Alexandra; BRABEC, Marek; MUSIL, Vladimír; ZACH, Petr. Morphology of Anterior Cingulate Cortex and Its Relation to Schizophrenia. *Journal of Clinical Medicine*. 2023, **12**(1), 33. ISSN 2077-0383. DOI: 10.3390/jcm12010033.

IF: 4.964/2021 (Q2/2021)

Co-author

2. ZACH, Petr; BARTOŠ, Aleš; LAGUTINA, Anastasiya; WURST, Zdeněk; GALLINA, Pasquale; RAI, Tanya; KIESLICH, Karel; RIEDLOVÁ, Jitka; IBRAHIM, Ibrahim; TINTĚRA, Jaroslav; MRZÍLKOVÁ, Jana. Easy identification of optimal coronal slice on brain magnetic resonance imaging to measure hippocampal area in Alzheimer's disease patients. *BioMed Research International*. 2020, (September), 5894021. ISSN 2314-6133. DOI: 10.1155/2020/5894021.

IF: 3.411/2020 (Q2/2020)

3. WURST, Zdeněk; BIRČÁK KUCHTOVÁ, Barbora; KŘEMEN, Jan; **LAHUTSINA, Anastasiya**; IBRAHIM, Ibrahim; TINTĚRA, Jaroslav; BARTOŠ, Aleš; BRABEC, Marek; RAI, Tanya; ZACH, Petr; MUSIL, Vladimír; OLYMPIOU, Nicoletta; MRZÍLKOVÁ, Jana. Basal ganglia compensatory white matter changes on DTI in Alzheimer's disease. *Cells*. 2023, **12**(April), 1220. ISSN 2073-4409. DOI: 10.3390/cells12091220.

IF: 7.666/2021 (Q2/2021)

9.1 Original scientific papers *in extenso* without relation to the topic of the dissertation

4. GAŠPAR, Branislav; MRZÍLKOVÁ, Jana; HOZMAN, Jiří; ZACH, Petr; **LAHUTSINA, Anastasiya**; MOROZOVA, Alexandra; GUARNIERI, Giulia; RIEDLOVÁ, Jitka. Micro-Computed Tomography Soft Tissue Biological Specimens Image Data Visualization. *Applied Sciences*. 2022, **12**(10), 4918. ISSN 2076-3417. DOI: 10.3390/app12104918.

IF: 2.838/2021 (Q2/2021)